FORSCHUNGSZENTRUM ROSSENDORF FZR/4K

WISSENSCHAFTLICH-TECHNISCHE BERICHTE
**FZR-298**
August 2000
ISSN 1437-322X



*Gudrun Müller und Jürgen Böhmert*

# Metallographic Post-Test Investigations for the Scaled Core-Meltdown-Experiments FOREVER-1 and -2

Herausgeber:
FORSCHUNGSZENTRUM ROSSENDORF
Postfach 51 01 19
D-01314 Dresden
Telefon +49 351 26 00
Telefax +49 351 2 69 04 61
http://www.fz-rossendorf.de/

Als Manuskript gedruckt

FORSCHUNGSZENTRUM ROSSENDORF
WISSENSCHAFTLICH-TECHNISCHE BERICHTE
**FZR-298**
August 2000

*Gudrun Müller und Jürgen Böhmert*

# Metallographic Post-Test Investigations for the Scaled Core-Meltdown-Experiments FOREVER-1 and -2

## Abstract

FOREVER (Failure Of Reactor Vessel Rentention) experiments have been carried out in order to simulate the behaviour the lower head of a reactor pressure vessel under the conditions of a depressurized core melt down scenario. In particular the creep behaviour and the vessel failure mode have been investigated. Metallographic post test investigations have complemented the experimental programme. Samples of different height positions of the vessel of the FOREVER-C1 and -C2 experiments were metallographically examined and characteristic microstructural appearances were identified. Additionally samples with uneffected microstructure were annealed at different temperatures and cooled by different rates and afterwards investigated. In this way the microstructural effects of the temperature regime, the thermomechanical loads and the environmental attack could be characterized. Remarkable effects were characteristic for the FOREVER-C2 experiment where the highest-loaded region below the welding joint reached temperatures of approx. 1100°C and a strong creep damage occured. In the FOREVER-C1 experiment creep damage could not be observed and the maximum temperature did not exceed 900°C. Environmental attack generated decarburization and oxidation but the effect was restricted to a narrow surface layer. There was almost no chemical interaction between the oxidic melt and the vessel material.

## Acknowledgements

The FOREVER-C1 experiment was performed under the partial sponsorship of EU. The FOREVER-C2 experiment was performed under the sponsorship of the APR, Project of the SKI, Swedish and Finish Power Companies, USNRC, and HSK.
The authors are grateful to R. Opitz for the careful carrying out of the metallographic preparation and photographics and to H.-G. Willschütz for the qualified introduction in the FOREVER experiment.

## Contents

## 1. Introduction

The development of an in-vessel melt retention strategy in the case of low-pressure core melt accidents could be an essential step for the further improvement of severe accident management measures. As a contribution to this the FOREVER (Failure Of REactor VEssel Retention) experimental programme has been initiated at the Division of Nuclear Power Safety of Royal Institute of Technology (RIT/NPS, Stockholm, Sweden) [1]. The programme is part of the EU MVI (Melt-Vessel Interactions) project. With these experiments the behaviour of the lower head of the reactor pressure vessel (RPV) under the thermal loads of a convecting melt pool with decay heating and under the pressure loads of a depressurization accident scenario is to be simulated.

The FOREVER programme consists of three phases. During the first series of experiments (FOREVER-C) the creep behaviour and the vessel failure mode are investigated. The main component of the FOREVER-C test facility is a 1:10 scaled version of the lower head of a prototypical light water reactor pressure vessel. Characteristic dimensions of the FOREVER vessels are an outer radius of 195 mm, a height of 600 mm and a wall thickness of 15 mm. With the experimental setup three effects can be stimulated: a) the reaction with the melt by pouring of approx. 15 ltrs. binary oxidic $CaO$-$B_2O_3$ melt, b) the internal decay heat generation by means of a resistance heater fixed within the vessel, and c) the internal pressure load by a pressurization system with ballons containing pressurized argon gas. The facility is equipped by a sophisticated instrumentation system to measure temperature, pressure and wall deformation.
Additionally, the experiments are accompanied by numerical calculations with different codes. In particular, a thermomechanical analysis is developed on the basis of a FE model using the commercial code ANSYS/Multiphysics, [2].

Complementing the working programme metallographic post-test investigations have been added. The benefit of such investigations is manifold.
On the one hand, the metallographic investigations provides insights into the material processes during the testing phase. Firstly, damage mechanisms due to environmental effects, e.g. reactions between melt and vessel, are revealed. Secondly, the evolution of creep damage can be identified and so the residual life time can be estimated. Eventually, changes of the microstructure give some information about the temperature regime. This is above all useful if the measuring sensors partly or completely fail as happened in the FOREVER-C1 and -C2 experiment. However, for a such complex material system like reactor pressure vessel steel the microstructural state at room temperature is a complicated, ambiguous function not only of the temperature but also the time, the heating and cooling rate and even the initial state. Therefore, the microstructural investigation will not more provide than temperature limits which were attained or exceeded.
On the other hand, the investigation contribute to the expert's knowledge on the material behaviour during a core melt accidents needed for reconstructing of the accident sequence as is exemplified by the TMI accident. In this case of TMI accident, afterward an extended research programme was required in order to produce this expert's knowledge.

The paper reports results obtained with samples from the vessel of the FOREVER-C1 and -C2 experiments. In these experiments external wall temperatures of 700 – 800°C in FOREVER-C1 and 950 - 1000°C in FOREVER-C2 were measured and, thus, changes of the microstructure can be expected.
Regarding to a detailed description of the experimental setup, the sequences and the results of the experiments the reader is referred to [1-4].

## 2. Material, Processing and Testing Conditions

Only few data are known about the pressure vessel material and its processing. The vessel was fabricated from two parts. The upper cylindrical part is a standard tube made from the German DIN 15 Mo 3 steel. The composition and the mechanical properties are given in Tables 1 and 2.

Table 1: Chemical composition of the DIN 15 Mo 3 steel [1] (in wt.-%)

| C | Si | Mn | P | S | Al | Mo | Ni |
|---|---|---|---|---|---|---|---|
| [%] | [%] | [%] | [%] | [%] | [%] | [%] | [%] |
| 0,12 - 0,20 | ≤ 0,35 | 0,4 - 0,9 | ≤ 0,03 | ≤ 0,025 | - | 0,25 - 0,35 | ≤ 0,3 |
| 0,16 | 0,17 | 0,62 | 0,009 | 0,011 | 0,021 | 0,28 | - |

Table 2: Mechanical properties of the DIN 15 Mo 3 steel according to the manufacturers data [1]

| | | |
|---|---|---|
| Yield point | ≥ 270 | [N/mm²] |
| Tensile Strength | 450 - 600 | [N/mm²] |
| Elongation | 20 | [%] |
| Brinell Hardness | 150 - 160 | |
| Test temperature | 20 | [°C] |

The lower head of the vessel has a hemispherical form and was manufactured from a rolled plate by hot-pressing. For the FOREVER-C1 experiment a plate from the same steel like the cylindrical part was used whereas the lower part of the FOREVER-C2 vessel was manufactured from the French 16 MND 5 steel. Its nominative chemical composition is quoted in Table 3.

Table 3: Chemical composition of the 16 MND 5 steel [3] (in wt.-%))

| C | Si | Mn | $P_{max}$ | $S_{max}$ | Cr | Mo | Ni |
|---|---|---|---|---|---|---|---|
| [%] | [%] | [%] | [%] | [%] | [%] | [%] | [%] |
| 0,25 | 0,15 – 0,3 | 1,15 - 1,5 | 0,035 | 0,040 | - | 0,45 – 0,6 | 0,4 - 0,7 |

Both parts of the vessels were joint by welding and afterwards stress relief annealed with the parameters 590 – 600°C/1h, heating rate 90K/h and cooling rate 100 K/h, [5]. The facility has been tested in accordance with Swedish Regulations AFS 1994:39, TKN 1987 [3].

For the German DIN 15 Mo 3 steel the CCT diagram (continuous cooling transformation) is known and depicted in Fig. 1 [6]. This diagram describes the transformation of the microstructure during continuous cooling from the austenite phase field. It also includes the transformation temperatures $A_{c1}$ (730°C – 750°C) and $A_{c3}$ (850°C – 865°C). At temperatures above $A_{c3}$ the microstructure is austenitic. The temperature range between $A_{c3}$ and $A_{c1}$ is the range of transformation, at temperatures below $A_{c1}$ the microstructure consists of ferrite/perlite or bainite (or mixture of them respectively), depending on the cooling rate and the temperature.

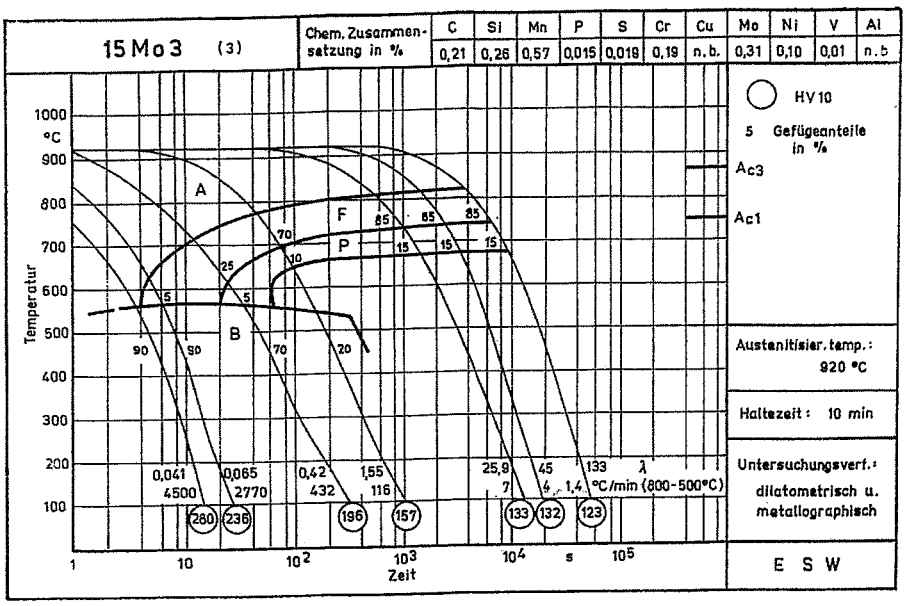


Fig.1: CCT diagram of 15 Mo 3 steel [6]

The authors is not available a CCT diagram of the French 16 MND 5 steel. It can be assumed that the transformation behaviour of the French 16 MND 5 steel (including the transformation temperatures) is comparable to the German 20 MnMoNi 5 5 reactor pressure vessel steel due to the similar chemical composition. Fig. 2 shows the CCT diagram of 20 MnMoNi 5 5 steel. In comparison with the 15 Mo 3 steel the ferrite-perlite transformationis delayed and the range of bainitic transformation is extended .

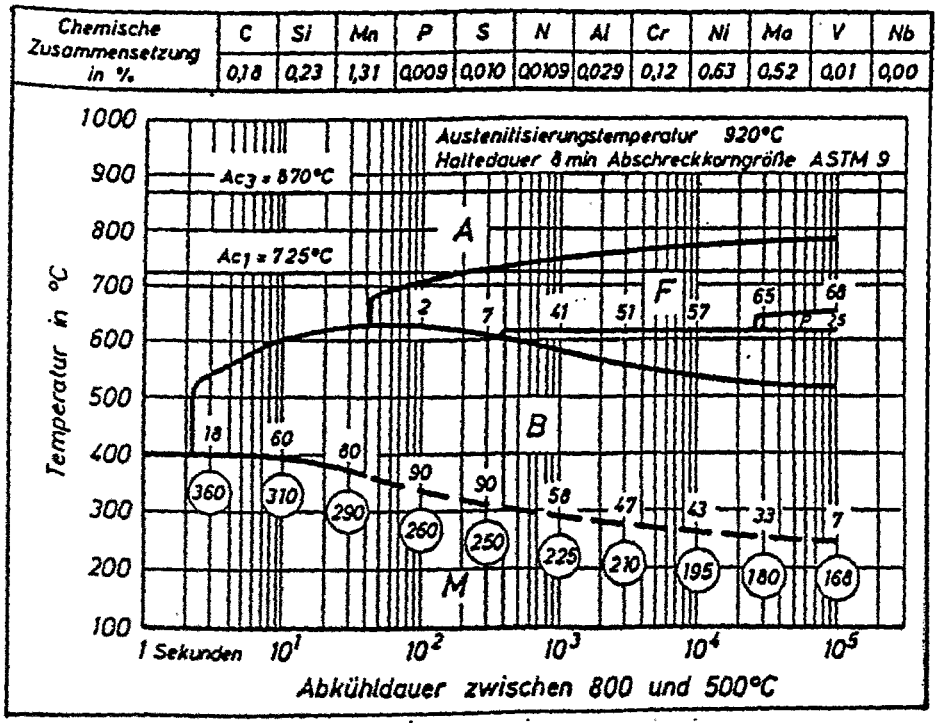


Fig. 2: CCT diagram of 20 MnMoNi 5 5 [7]

The oxidic $CaO-B_2O_3$ mixture used is an aggressive melt (C1: 20 % CaO, 80 % $B_2O_3$, C2: 30 % Ca0, 70 % $B_2O_3$). Measurements of the thermophysical properties of a 30-70 a/c mixture were performed in the Institute of Silicate Research St. Petersburg (Russia) and GLAFO company (Stockholm, Sweden). Together with the phase diagram of this binary system the properties are given in [3].

The loading sequences and some measuring results are summerized in Table 4. In both cases the vessel was preheated ($T_o$), than the melt ($T_{melt}$) prepared outside the vessel poured into the vessel and the internal heater was adjusted to the heating power (Q) requested. After a waiting period to achieve the thermal balance, the vessel was pressurized ($p_i$).

Table 4: Experimental conditions of FOREVEVER-C1 and -C2

| Exp.-Nr. | $T_o$ / °C | $p_i$ / MPa | $T_{melt}$ / °C | Q / kW | $T_{ext}$ / °C [1] | Dura-tion/h [2] | Com-ments |
|---|---|---|---|---|---|---|---|
| C1 | 400 | 2 | 1050...1100 | 22 | < 800 | 28/21 | |
| C2 | 800 | 25...28 | 1200 | 40 | 960 | 10/5 | heater failure |

1) $T_{ext}$ – external wall temperature maximally measured
2) First figure: total duration, second figure: thermal steady state

## 3. Investigation Program and Sampling

The following investigations are focussed on the analysis of the microstructural evolution within the vessel wall during the FOREVER-C1 and FOREVER-C2 experiment. For this investigations one segment of the hemispherical part of the vessel reaching from the bottom up to the weld and another from the cylindrical part including the weld were available. Furthermore a sample of the 16 MND 5 steel of another manufacturing series was investigated.

The investigation program consists in metallographic examinations of samples of the hemispherical part, of the weld, of the cylindrical part near the weld and of the $CaO-B_2O_3$ mixture.

For supplementary considerations annealing experiments with subsequent microstructural investigations were also carried out. Additionally, scanning electron microscope investigations and microhardness measurements were performed. A selected sample was analysed by the ion-microprobe method.

## 3.1 Sampling

The samples of FOREVER-C1 designated C1/1 to C1/6 and C1/A to C1/D were taken from the hemispherical bottom and the sample C1/S from the welding seam and the cylindrical part of the vessel. The samples of FOREVER-C2 designated C2/1 to C2/6, C2/A to C2/D and C2/S were taken by analogy with that. Fig. 3 shows the scheme of sampling.

FOREVER-C1 FOREVER-C2

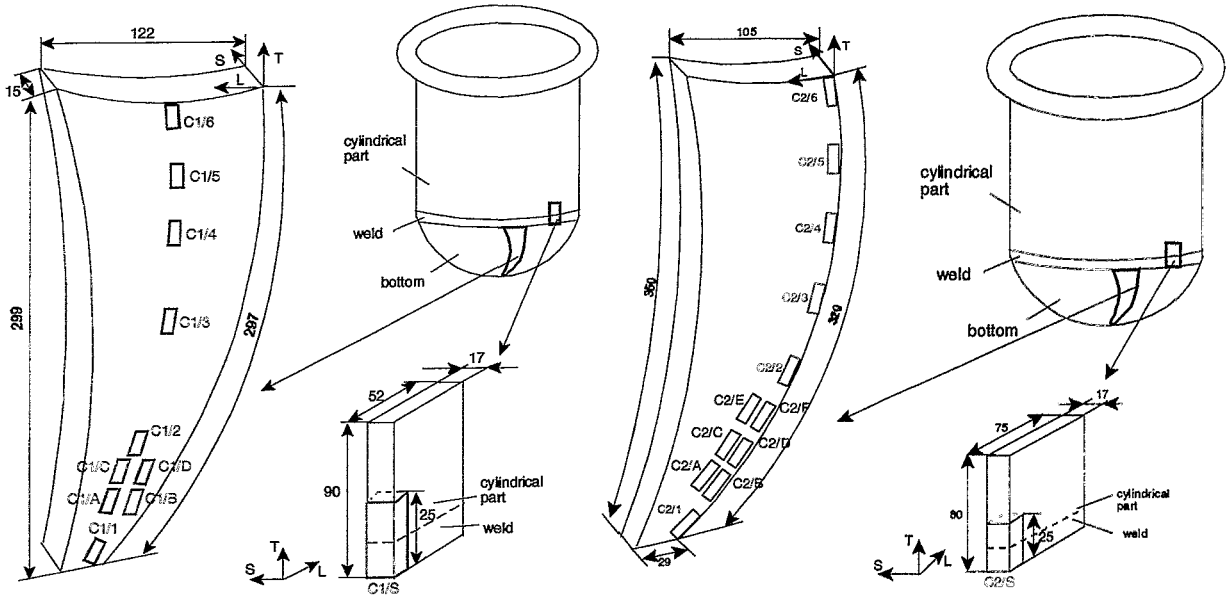


Fig. 3: Sampling of the hemispherical part and the cylindrical part with weld

## 3.2 Metallographic Investigations

Cross sections were made parallel to the S–T–plane (Fig. 3) of all samples to show the microstructure of the vessel wall from the inside to the outside. The samples were conventionally grinded and polished and finally etched with alcoholic 2 % nitric acid for 15 seconds.
For the metallographic examination an optical microscope (MEF4A) was used.

## 3.3 Annealing Experiments

In addition to the metallographic examination annealing experiments were carried out. The comparison between the microstructure after annealing and the vessel wall samples allows to draw conclusions about the temperature regime within the vessel wall. The material near positions C1/1 and C1/2 or C2/1 and C2/2 respectively is considered to be not affected by the FOREVER-C tests and represents the state after processing. Always two samples from the position between C1/1 and C1/2 respectively C2/1 and C2/2 (Fig. 3) were annealed at the same temperature for 2 h and subsequently cooled with two different cooling rates. The two different cooling rates were chosen as the microstructure also depends on the cooling rate. The cooling rate designated "furnace" approximately simulated the cooling rate of the FOREVER-C1 and FOREVER-C2 experiments. Table 5 presents an overview on the annealing experiments.

Table 5: Annealing Experiments

| Annealing Program | Sample | Temperature [°C] | Cooling | Cooling Procedure |
|---|---|---|---|---|
| G 1.1 | C1/A | 700 | Furnace | to 400°C/1h; to 100°C/2h |
| G 1.2 | C1/B | 700 | Air | |
| G 2.1 | C1/C | 800 | Furnace | to 400°C/1h; to 100°C/2h |
| G 2.2 | C1/D | 800 | Air | |
| G 3.1 | C1/A | 900 | Furnace | to 500°C/1h; to 300°C/1h; to 100°C/2h |
| G 3.2 | C1/B | 900 | Air | |
| G 4.1 | C1/C | 1050 | Furnace | to 600°C/1h; to 400°C/1h; to 100°C/2h |
| G 4.2 | C1/D | 1050 | Air | |
| G 5.1 | C2/A | 800 | Furnace | to 400°C/1h; to 100°C/2h |
| G 5.2 | C2/B | 800 | Air | |
| G 6 | C2/E | 850 | Furnace | to 350°C/2h; to 200°C/1h |
| G 7 | C2/F | 900 | Furnace | to 400°C/2h; to 200°C/2h |
| G 8.1 | C2/C | 950 | Furnace | to 500°C/1h; to 300°C/1h; to 100°C/2h |
| G 8.2 | C2/D | 950 | Air | |
| G 9.1 | C2/B | 1050 | Furnace | to 500°C/1h; to 300°C/1h; to 100°C/2h |
| G 9.2 | C2/A | 1050 | Air | |
| G 10.1 | C2/C | 1100 | Furnace | to 600°C/1h; to 400°C/1h; to 100°C/2h |
| G 10.2 | C2/D | 1100 | Air | |

### 3.4 Scanning Electron Microscope Investigations

The etched sample C2/3 was tested by the scanning electron microscope to analyse components of the microstructure. It was measured by a scanning electron microscope ZEISS DSM 962 (25 kV) with backscattering detector and the microanalysis system INCA (Oxford Instruments) for Energy Dispersive X-ray analysis (EDX).

### 3.5 Microhardness Measurements

The microhardness of the sample C2/6 was measured from the inside to the outside of the vessel wall with two different loads ( 0,471 N, 0,235 N ). Additionally, the microhardness of the sample C2/S was measured along a line from the base material into the weld.

### 3.6 Ion-Microprobe Analysis

The non-etched sample C1/4 was tested by the ion-microprobe to detect the diffusion of boron into the wall. It was measured by line scanning from the inside to the middle of the sample at two different positions. The main parameters of the Rossendorf 's Nuclear Microprobe [8] installed at the 3 MV-Tandetron are:

| | |
|---|---|
| Lens system: | electromagnetic quadrupole triplet |
| Refractive power: | M x E / $q^2$=45 MeV amu (atomic mass units) |
| Incidence particles: | protons, nearly all ions with Z > 2 |
| Beam current: | > 100 pA |
| Beam spot: | ≈ 2 µm |
| Scanning area: | up to 2 x 2 $mm^2$ |

### 3.7 Determination of the Area Fraction of Creep Pores

The area fraction of creep pores (only for samples from FOREVER-C2) was determined by the image processing system LUCIA D on the metallographic cross-section. The image processing system uses the image of a CCD camera installed at a light microscope (NEOPHOT 2, Carl Zeiss Jena).

## 4. Results of the FOREVER-C1 Experiment

### 4.1 Metallographic Examination

In Figs. 4-7 typical microstructure of the inside, the middle and the outside of the vessel wall cross section at different height positions (C1/1, -1/3, -1/4 and –1/6) are shown. Depending on the height position and depth location there are different microstructural appearances.

Over a large area of the vessel cross section the most typical microstructure is a banded structure of polygonal ferrite and perlite. In the lower part of the vessel head this microstructure is modified over a range extending from approx. the middle up to the outside of the wall. Here a kind of duplex ferrite grains consisting of coarse grains in a fine-grained matrix and banded perlite occurs (Fig. 4). At the inside there is a narrow zone (approx. 0,2 mm) with mainly ferrite. This zone spreads widely over the middle of wall with increasing height position. The ferrite is fine-grained and the perlite is not banded but irregularly distributed. In the upper height positions a layer of a thickness of 1 mm consisting of coarse-grained ferrite is at the wall outside.

The microstructure of the weld and the adjacent cylindrical part of the vessel is shown in Figs. 8-10. Fig. 8 depicts the macrostructure of the weld. One can see the different beads of the multi-pass welding technology, the heat affected zone (HAZ) and the base material of the upper vessel region. The weld (Fig. 9) consists of the typical solidification microstructure and contains columnar bainitic grains and isolated coarse ferritic inclusions. The microstructure of the HAZ (Fig. 9) is coarse bainite with partly banded perlite near the inside, fine-grained ferrite and partly banded perlite in the middle of the wall and coarse bainite near the outside.

As Fig. 10 shows the microstructure of the base metal is a mixture of mainly fine-grained polygonal ferrite and banded perlite. Near the inside as well as the outside there are narrow ferritic layers (0.1...0.3 mm) without perlite. The ferritic grains are partly coarsened. The ferritic layers disappear in a distance of 7.5 mm (inside) or 1 mm (outside) respectively from the fusion line.

Effects of the melt on the steel microstructure cannot be found. Only on the cross section C1/4 (Fig. 6) there is a narrow layer (20 µm) of ferritic grains arranged perpendicular to the inner wall surface. This phenomenon is characteristic for boron diffusion layers due to boriding.

An impression of the macrostructure of the wall in the S-T-plane presents Fig. 11. Macrographs of the wall are depicted for the height positions 1 to 6. The macrographs do not show details of the microstructure but the boundaries of the different microstructural zones can be identified in connection with Figs. 4-7. Above all, the broad zone consisting of ferrite and banded perlite, which occurs in all positions, can be recognized.
Fig. 12 summerizes the microstructural appearances in a map of the characteristic zones over the cross section of the vessel wall.

Inside

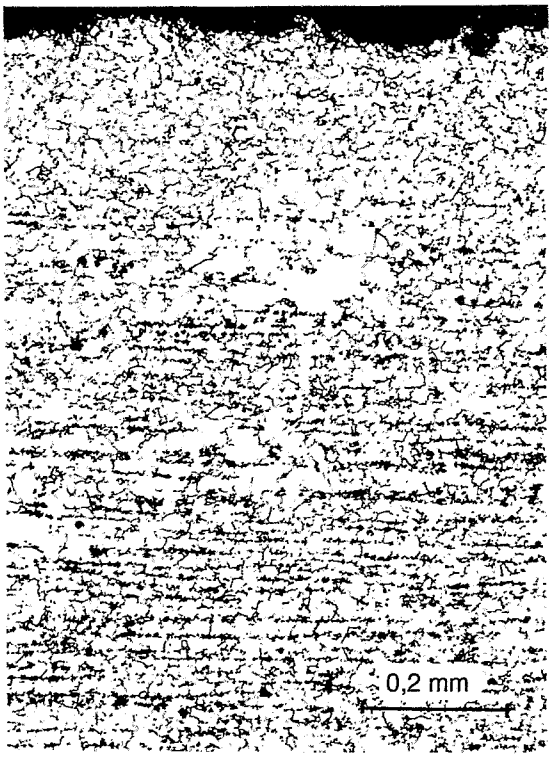


Middle

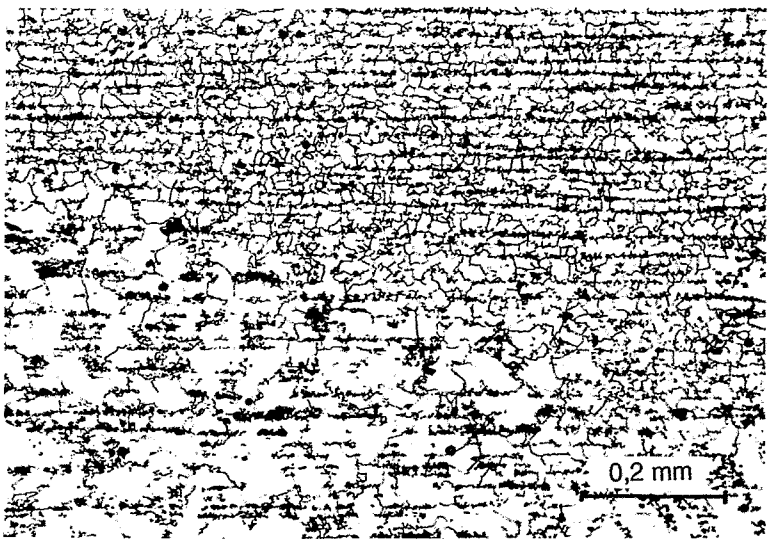


Outside

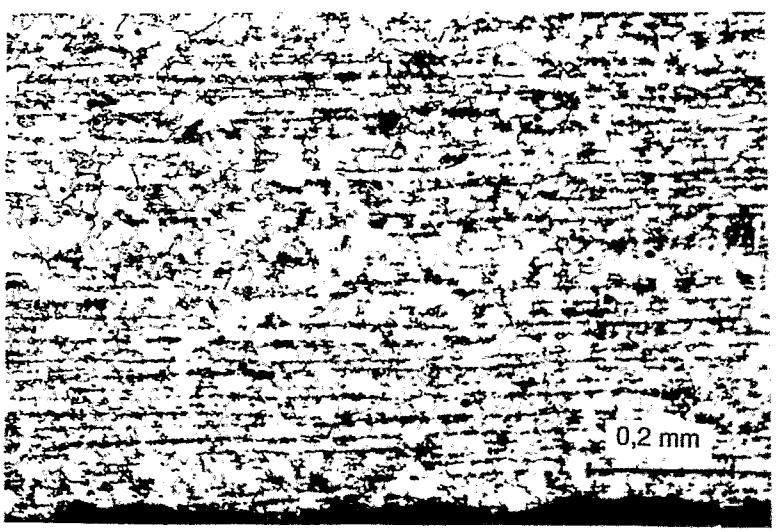


Fig. 4: Microstructure of sample C1/1, different locations over the wall thickness

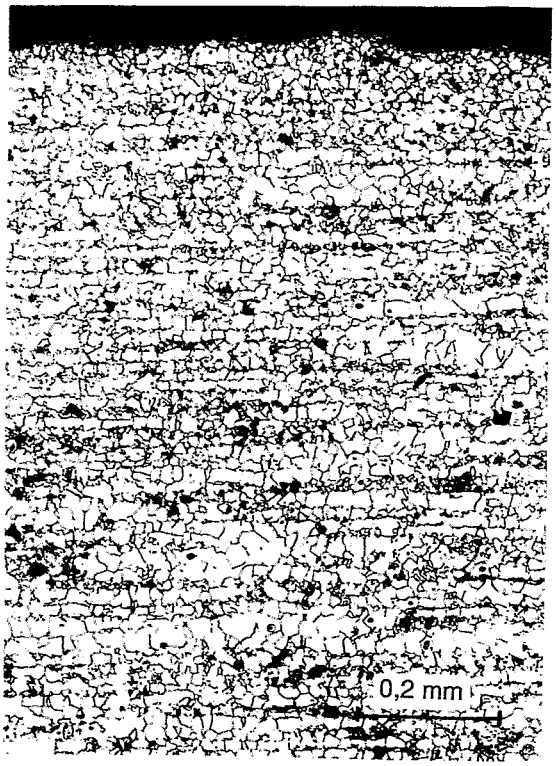


Inside

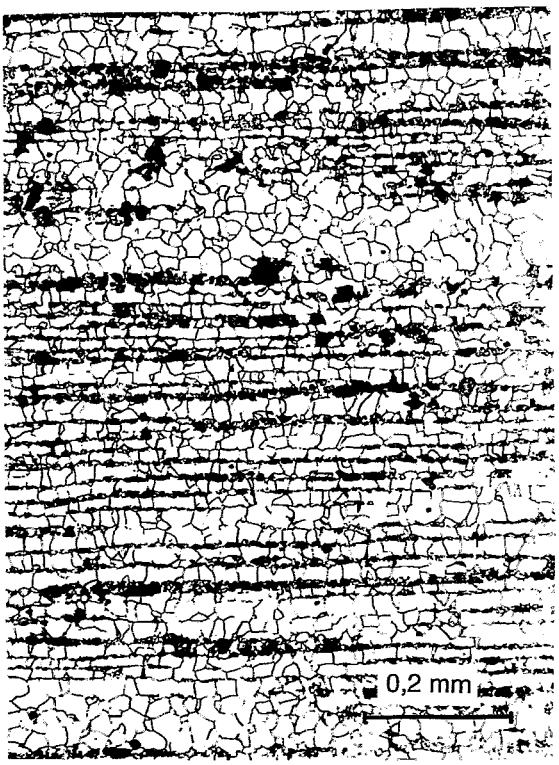


Middle

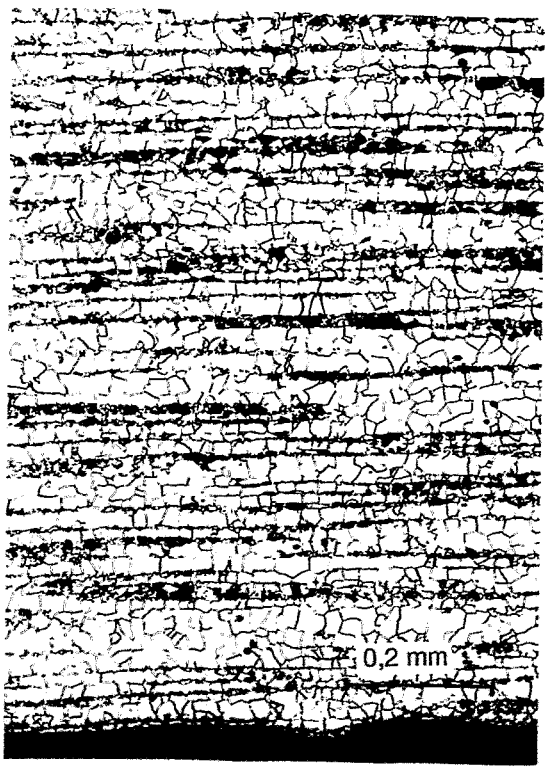


Outside

Fig. 5: Microstructure of sample C1/3, different locations over the wall thickness

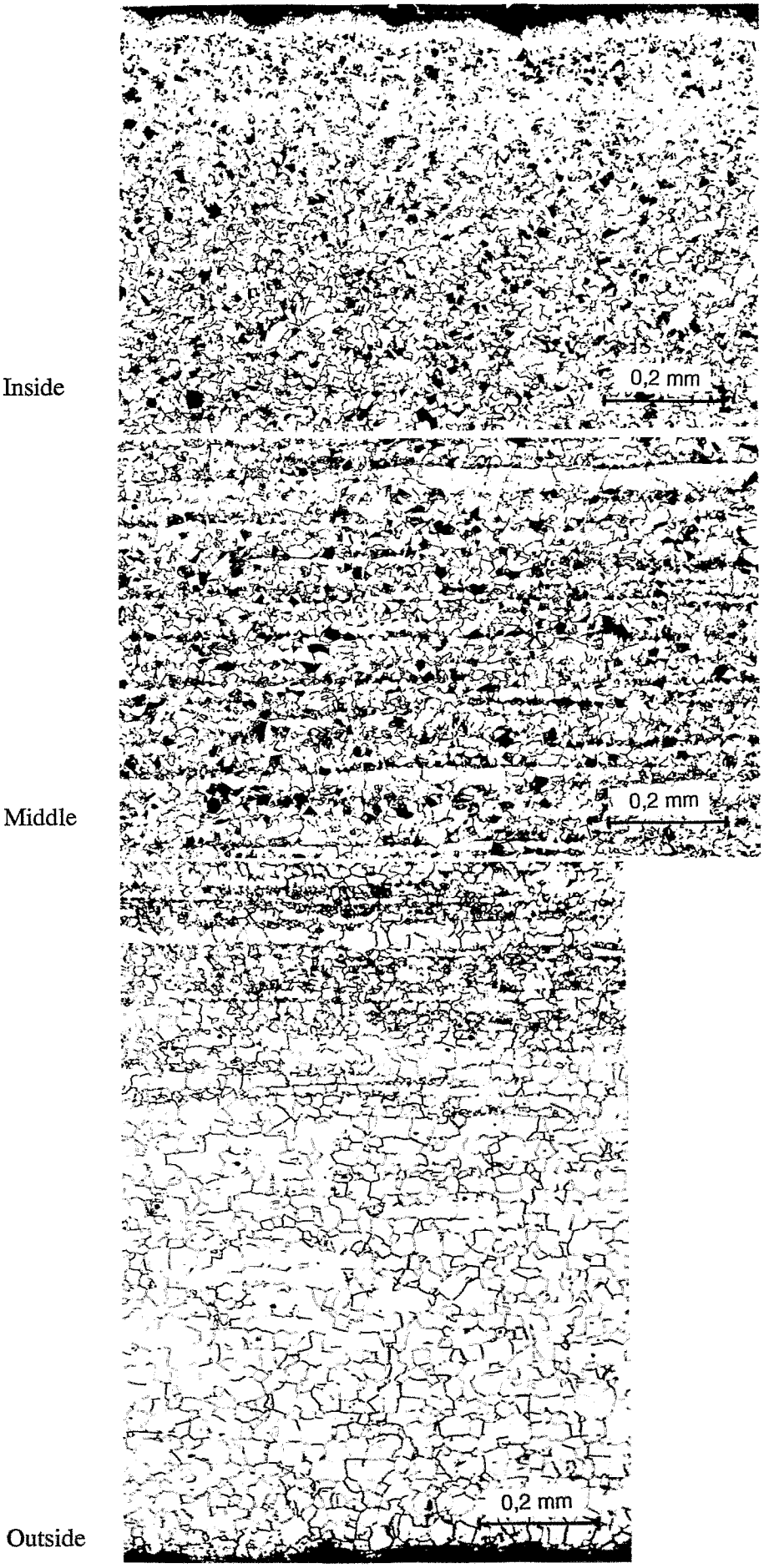


Fig. 6: Microstructure of sample C1/4, different locations over the wall thickness

Inside

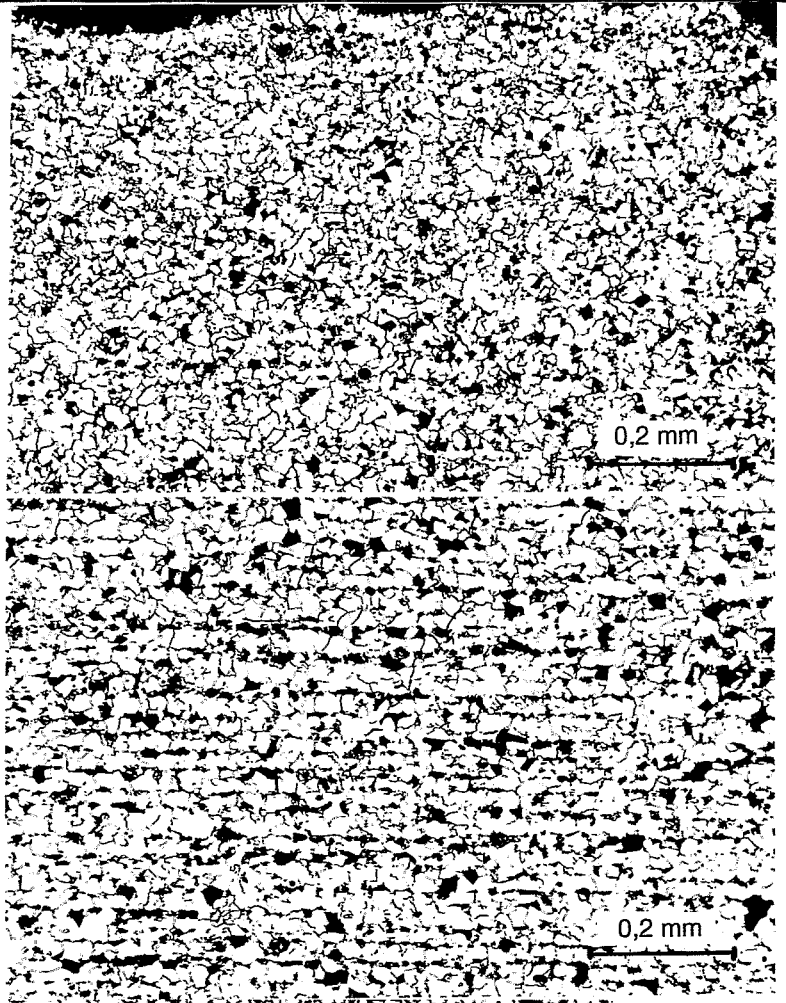


Middle

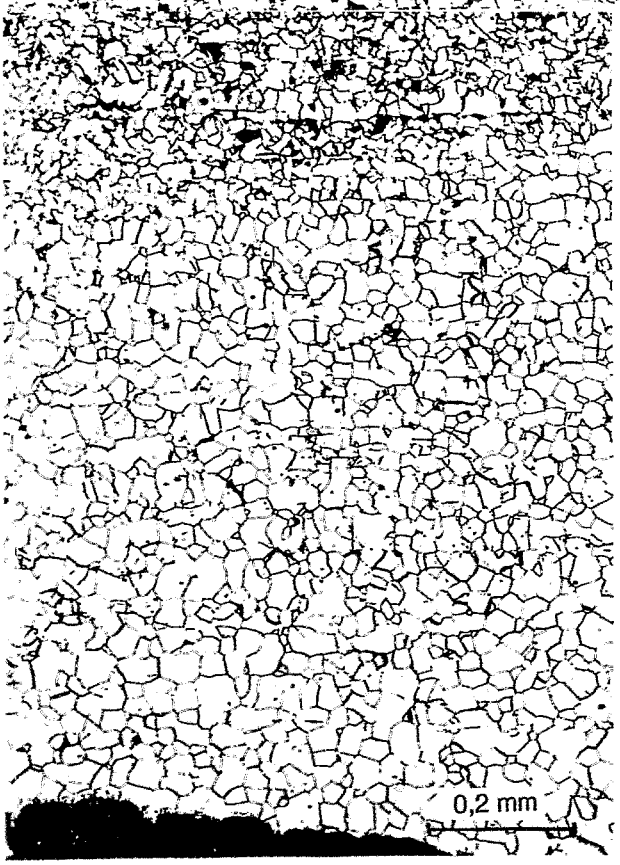


Outside

Fig. 7: Microstructure of sample C1/6, different locations over the wall thickness

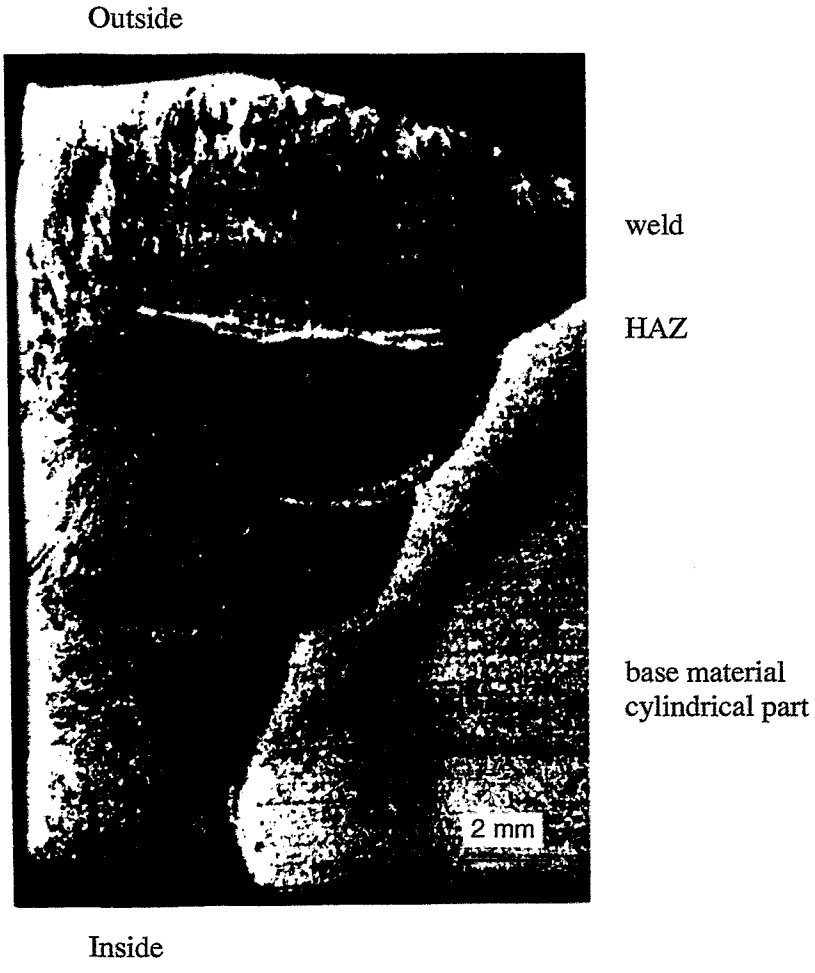


Fig. 8: Macrostructure of sample C1/S, weld and adjacent base material (cylindrical part of the vessel)

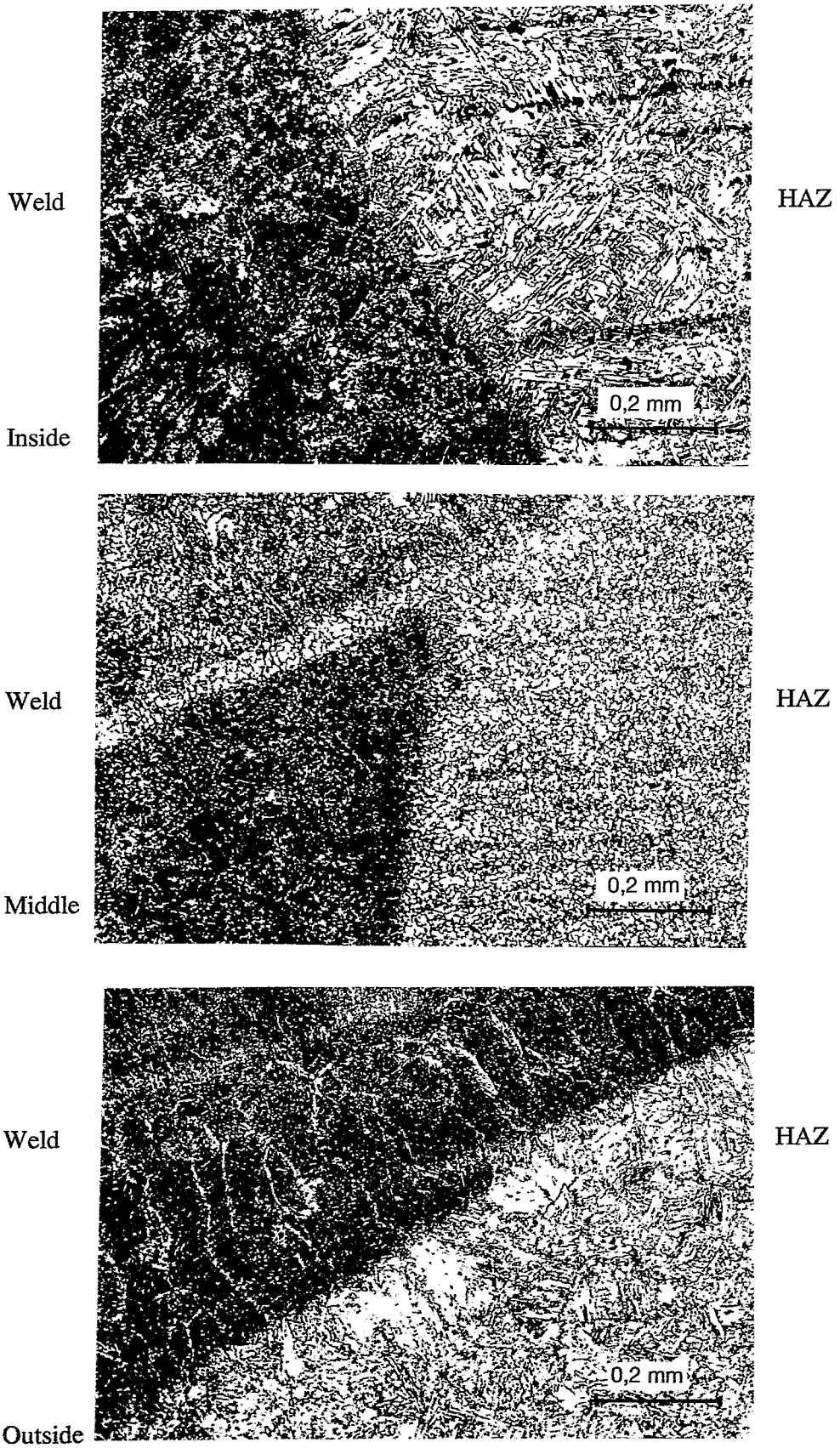


Fig. 9: Microstructure of sample C1/S, different locations over the wall thickness, weld and heat-affected zone (HAZ)

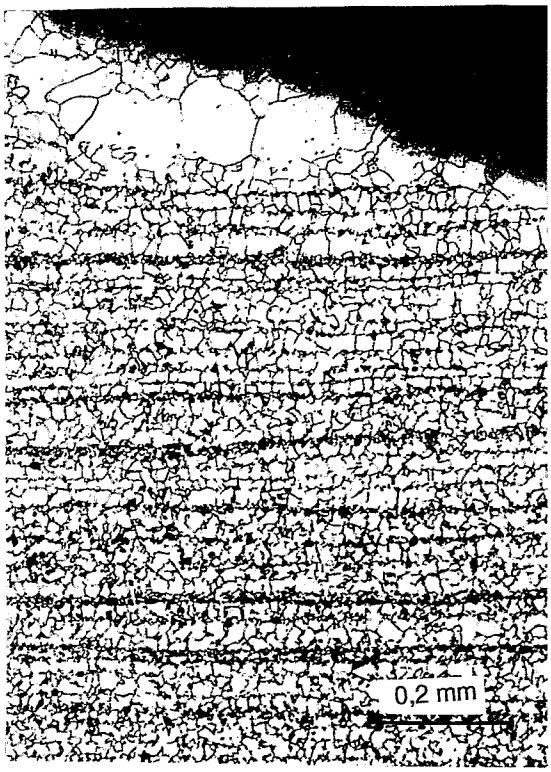


Inside

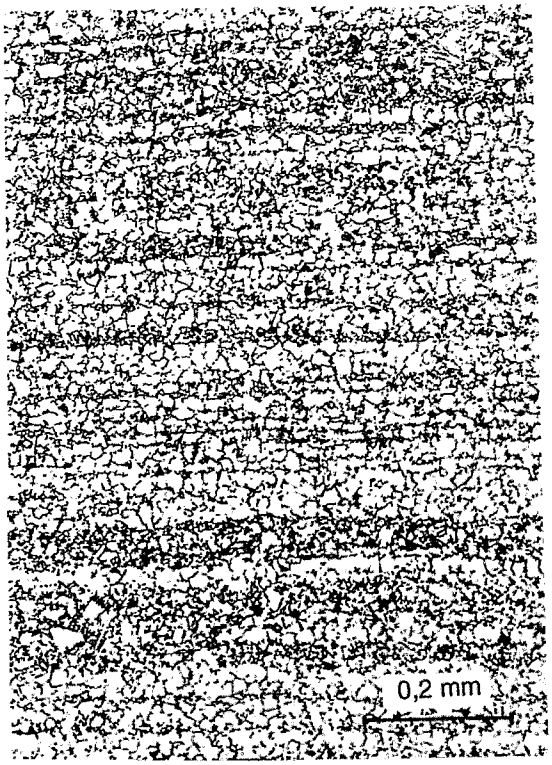


Middle

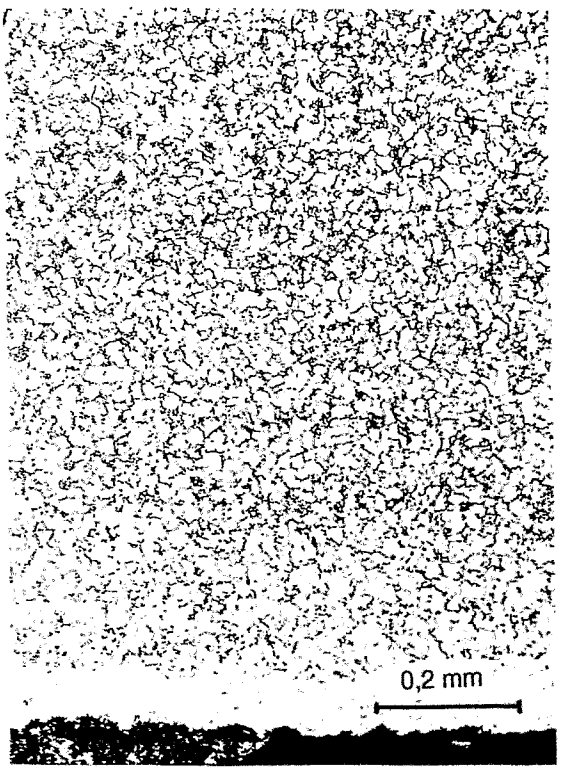


Outside

Fig. 10: Microstructure of sample C1/S, different locations over the wall thickness, base material of the cylindrical part near the weld

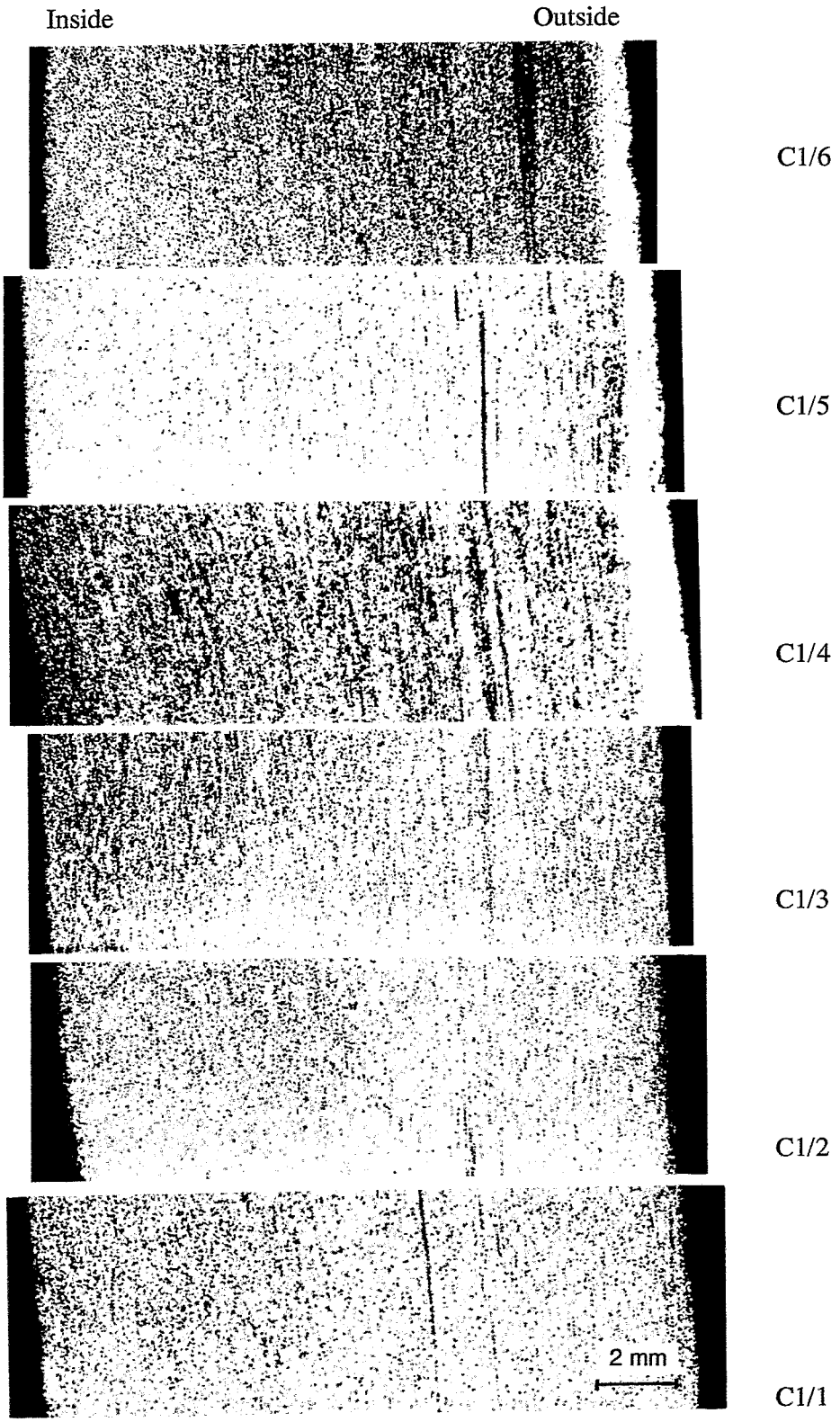


Fig. 11: Macrostructure of the hemispherical part of the vessel, FOREVER-C1

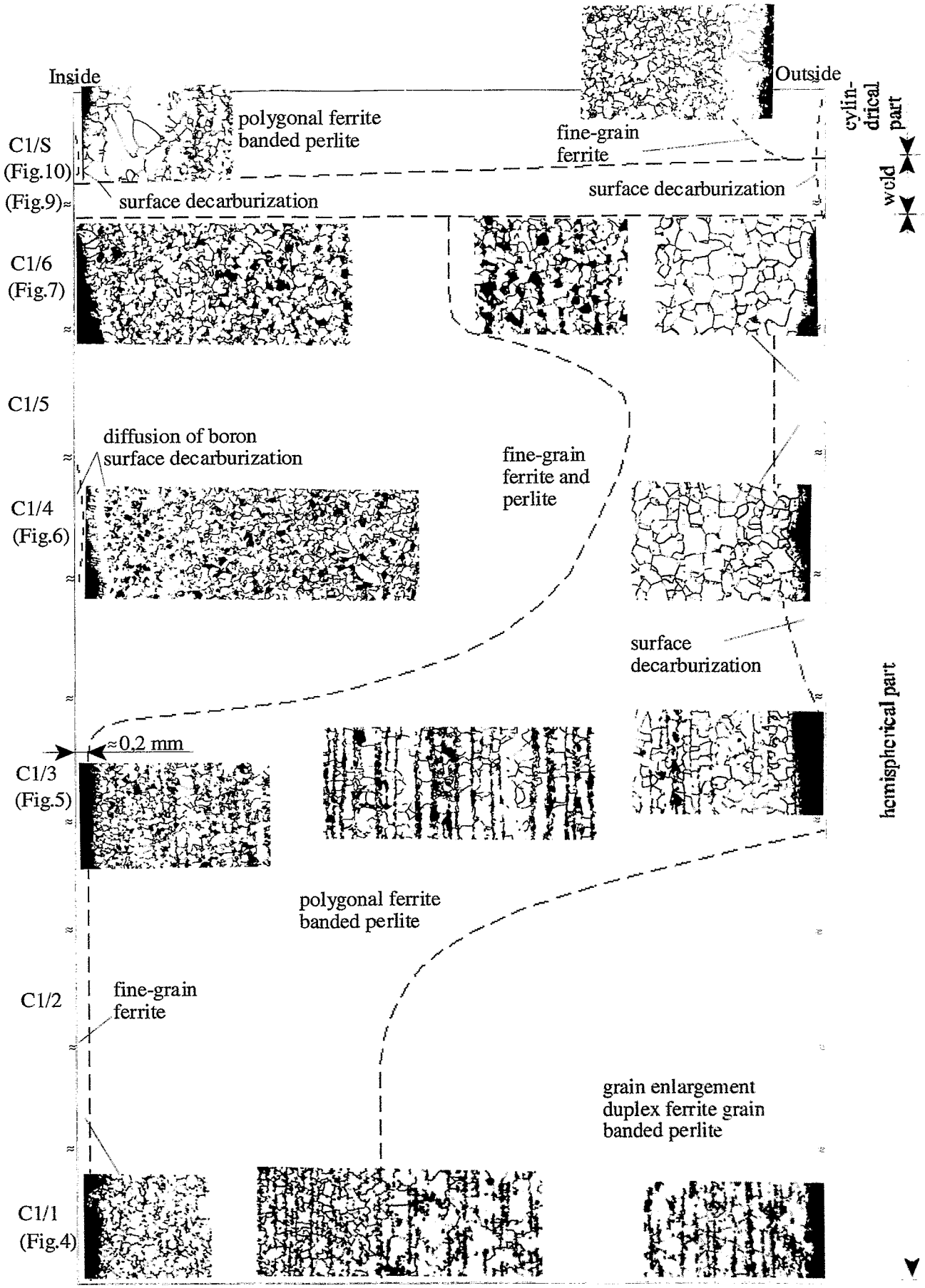


Fig. 12: Map of the characteristic zones of the microstructure of the vessel wall, FOR-EVER-C1 (scale of microstructures: 0,2 mm )

## 4.2 Microstructure after Annealing

The microstructure after annealing is shown in Figs. 13-20 according to the different annealing temperatures and cooling rates. The microstructure before annealing corresponds to the microstructure of samples C1/1 (Fig. 4) and C1/2. As already mentioned the microstructure is heterogeneous over the wall thickness and consists of fine-grained ferrite and perlite at the inside, polygonal ferrite and banded perlite near the middle and a ferrite-banded perlite mixture with coarse-grained ferrite cluster at the outside. Annealing at 700 °C (Figs. 13, 14) or 800 °C (Figs. 15, 16) does not change the initial microstructure. Firstly annealing at 900 °C (Figs. 17,18) modifies the initial microstructure. This is particularly visible after air cooling. In this case a mixture of polygonal ferrite, perlite and bainite occurs. The banded arrangement disappears (Fig. 18). After furnace cooling the mircrostructure contains polygonal ferrite and perlite which is only partly banded (Fig. 17). A clear effect shows annealing at 1050 °C (Figs. 19, 20). After furnace cooling a very coarse-grained microstructure consisting of polygonal ferrite and mainly banded perlite is created whereas after air cooling the most characteristic feature is a coarse bainite.

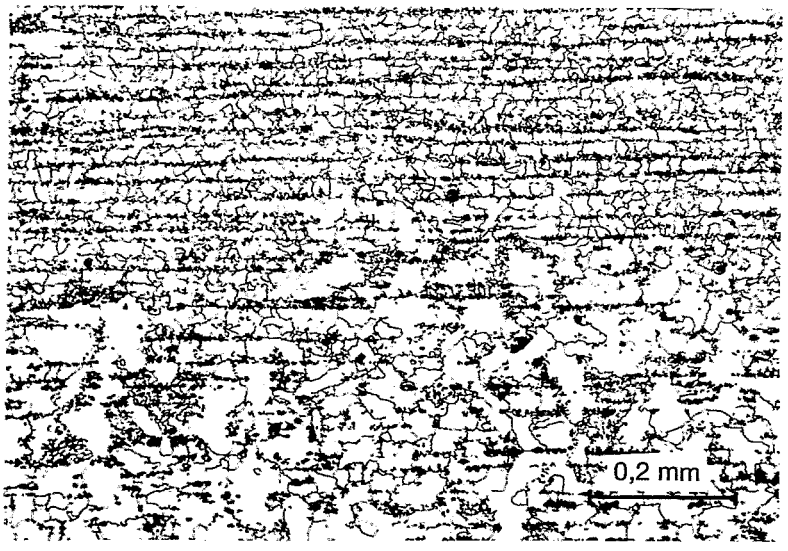


Fig. 13: Microstructure of sample C1/A, annealed: 700 °C/2 h, furnace cooling

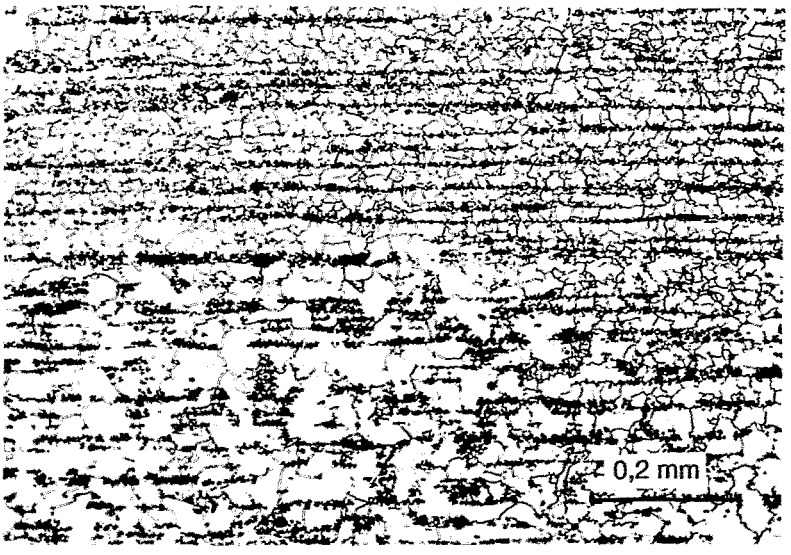


Fig. 14: Microstructure of sample C1/B, annealed: 700 °C/2 h, air cooling

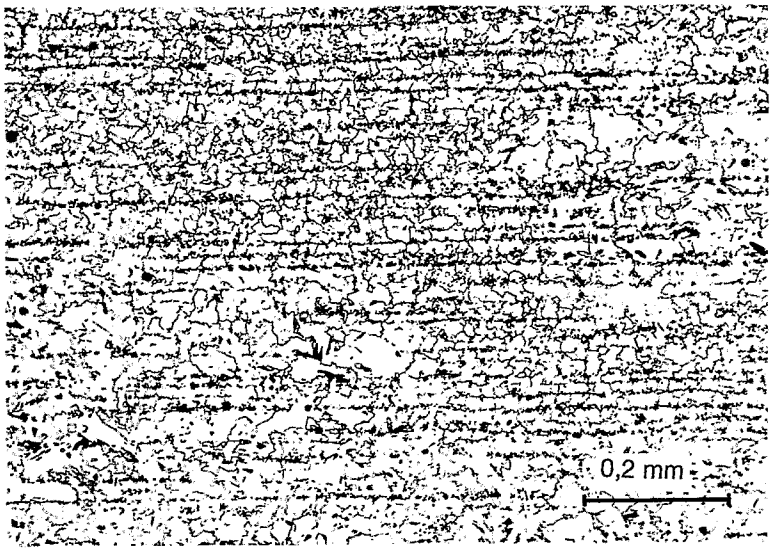


Fig. 15: Microstructure of sample C1/C, annealed: 800 °C/2 h, furnace cooling

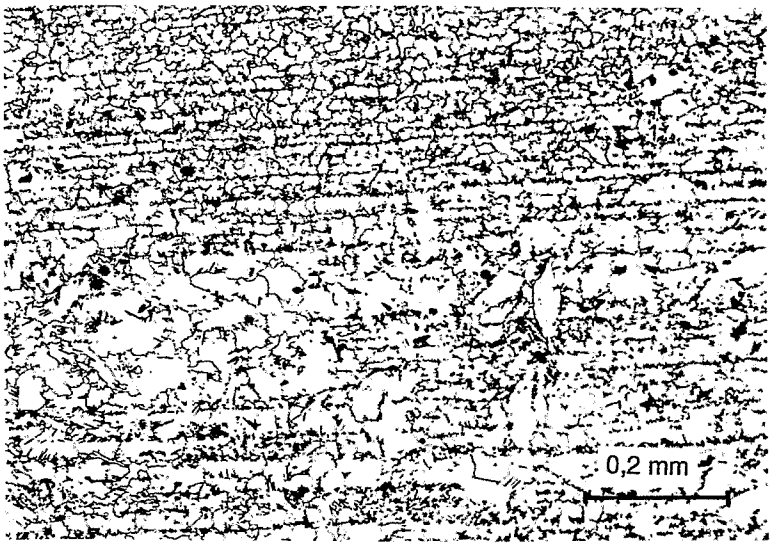


Fig. 16: Microstructure of sample C1/D, annealed: 800 °C/2 h, air cooling

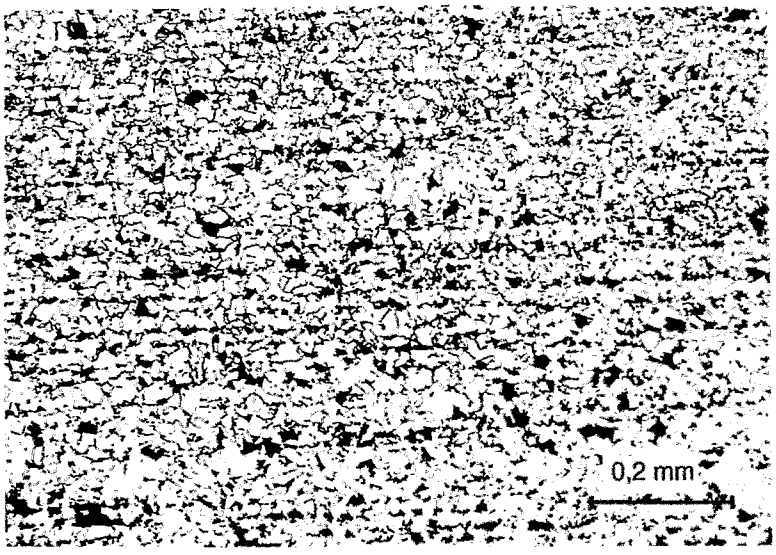


Fig. 17: Microstructure of sample C1/A, annealed 900 °C/2 h, furnace cooling

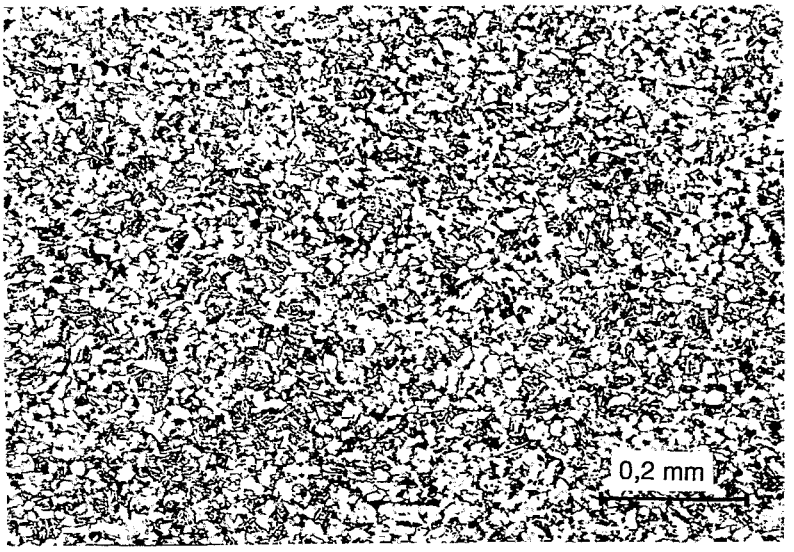


Fig. 18: Microstructure of sample C1/B, annealed: 900 °C/2 h, air cooling

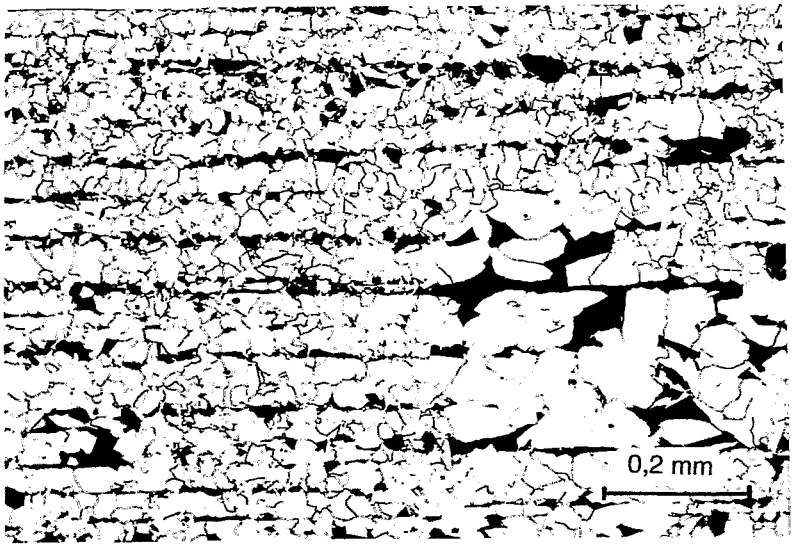


Fig. 19: Microstructure of sample C1/C, annealed: 1050 °C/2 h, furnace cooling

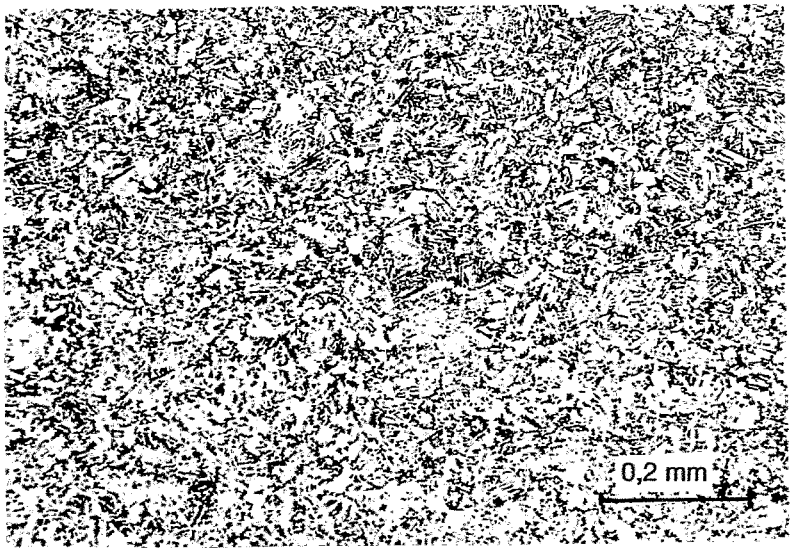


Fig. 20: Microstructure of sample C1/D, annealed: 1050 °C/2 h, air cooling

## 4.3 Ion-Microprobe Analysis

In the interior surface layer of sample C1/4, the diffusion of boron from the melt into the inside of the vessel was presumed. There the grains are arranged perpendicularly to the surface and a subsequent fine-grained decarburized layer is formed. The peripheral layer has a width of approx. 20 µm. In this layer an increase of the boron concentration by approx. 25 times compared to the boron concentration of the residual cross section was measured by the ion-microprobe method. Fig. 21 presents the course of the concentration of boron in dependence of the distance of the inner surface. From the result, a concentration of boron of 0,08 % in the diffusion layer is estimated. The width of this diffusion layer agrees very well with the light microscopic observation as shown in Fig. 22. At a further location of the same sample a diffusion zone of boron could not be clearly proved. The phenomenon was only observed at sample C1/4.

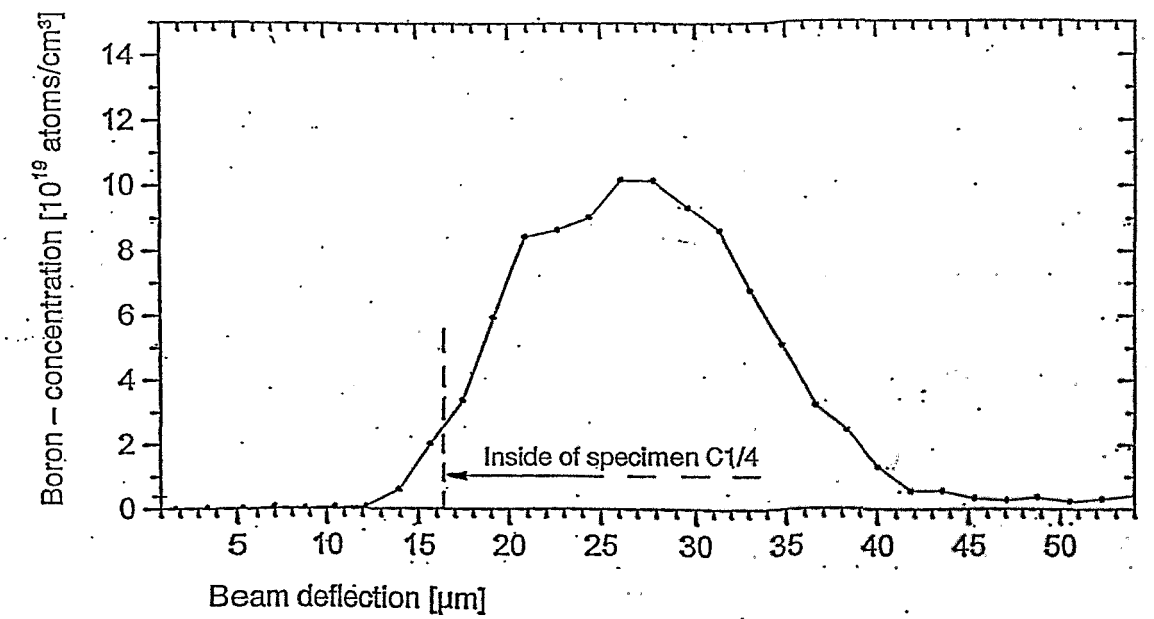


Fig. 21: Variation of the boron concentration with the distance, as determined by ion-microprobe technique

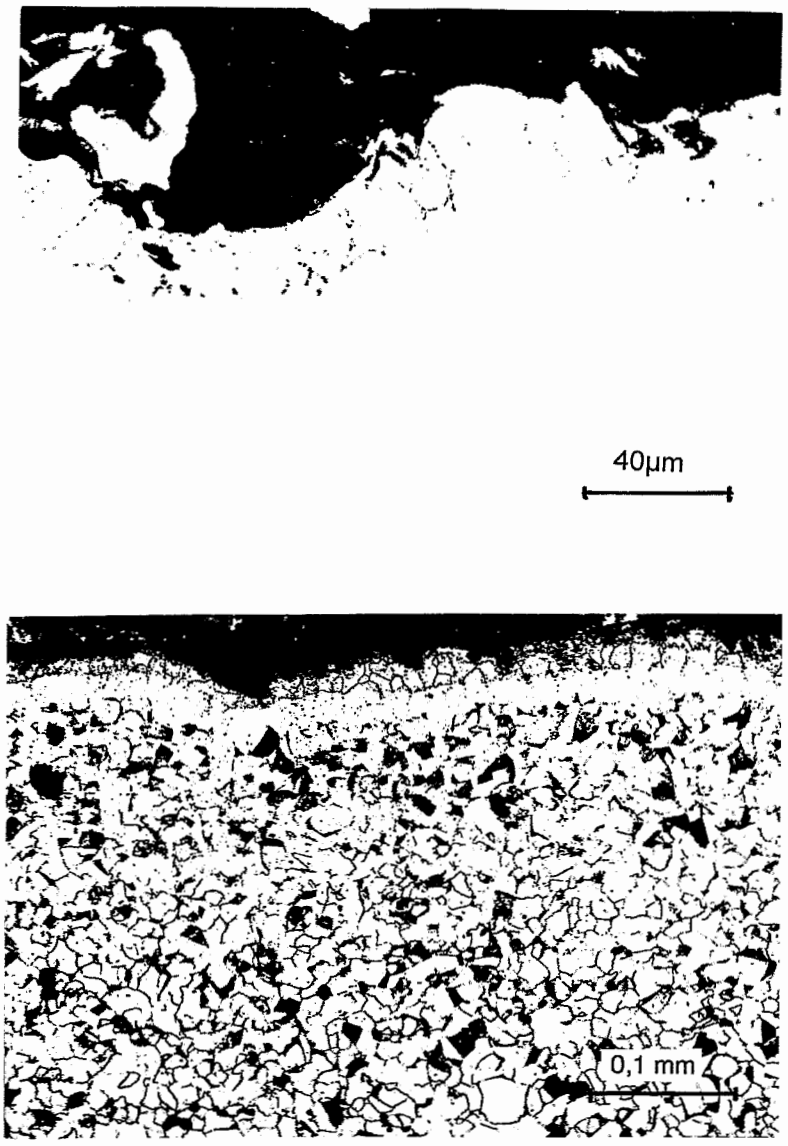


Fig. 22: Microstructure of sample C1/4, inside layer, non-etched (top) and etched (bottom)

# 5. Results of the FOREVER-C2 Experiment

## 5.1 Metallographic Examination

Optical micrographs of the cross section of the inside, the middle, and the outside of the vessel wall are shown for the different height positions in Figs. 23-27. The lower part (positions C2/1, C2/2) exhibits a quite homogeneous, fine bainitic microstructure containing a fraction of pre-eutectoid ferrite. Above all in the central part of the wall, there are so-called ghost lines, perceptible by the darker colouring in the micrographs. The ghost lines are produced by segregation of carbon and other alloy elements such as Mn and Mo.
Clearly different microstructure appears in the upper part of the vessel head. At the height position C2/3 the microstructure is a mixture of banded ferrite and perlite including isolated cluster of fine bainite or blocky ferrite. The nearer the location to the outside of wall the finer are the grains. Furthermore, at the outside a narrow surface layer of ferrite is formed. For the upper height positions, the content of perlite is reduced and the fraction of bainite is increased. At the inside a coarse lath-type of ferrite is formed (Figs. 25-27). The effect is particularly significant near the welding fusion line where this coarse bainite covers almost the total thickness. The residual wall thickness is covered by bands of ferrite in a bainitic matrix up to a narrow surface layer at the inside where polygonal ferrite is predominantly formed.

Fig. 28 presents the macrostructure of the weld. Here the different beads during multirun welding is hardly and the HAZ is not at all visible. The last one is confirmed by Fig. 29 which shows a sharp boundary line between the base metal of the hemispherical part of vessel and the weld. In the weld there is no typical solification structure. Instead of that a mixture of coarse-grained ferrite and perlite occurs.

The macrostructure of the 15 Mo 3 base metal of the cylindrical part of the vessel located near the weld is shown in Fig. 30. Predominantly, the microstructure consists in bands of coarse-grained ferrite and perlite. In this matrix, cluster of martensite-like structure are included. A narrow layer with martensite-like structure occurs at the inside. Near the outside the microstructure is a banded fine-grained ferrite-perlite mixture which is comparable with the microstructure of the C1/1 and C1/2 positions (Fig. 4) from the FOREVER-C1 experiment. Only at the outside, a ferritic layer without perlite is formed.

The unetched cross section reveals the appearance of pores. They appear on the outside of wall at the height position C2/4 at first, cover the whole cross section at the positions C2/5 and C2/6 and disappear for positions above the weld. The concentration of pores decreases with increasing distance of the outside up to the middle of wall and increases again to the inside on a lower level. Fig. 31 shows examples of the pore structure for the outside of position C2/6 and the welding seam. On the outside of position C2/6 the largest and already crack-like formed pores can be found. In the weld the pores are more numerous but smaller and spherically shaped.

An overview of the macrostructure of the lower part of vessel in the S-T-plane is shown in Fig. 32. Like Fig. 11 the figure does not show details of the microstructure but indicates the course of the characteristic microstructures. A summary of metallographic findings gives Fig. 33.

Inside

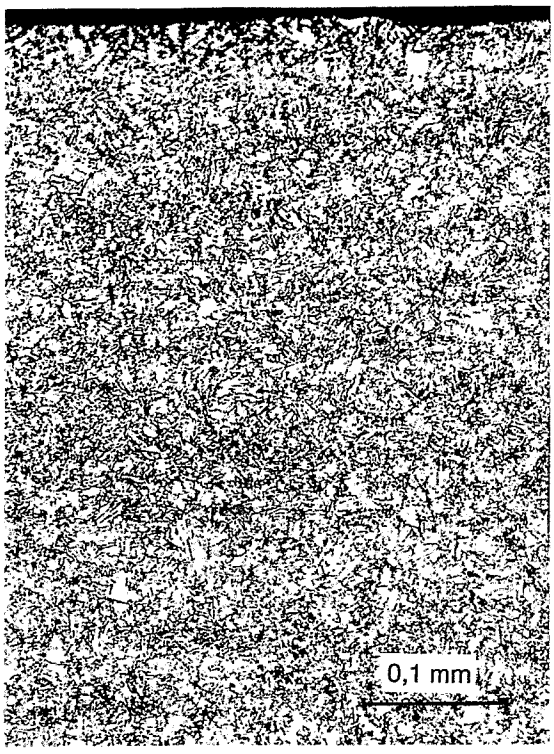


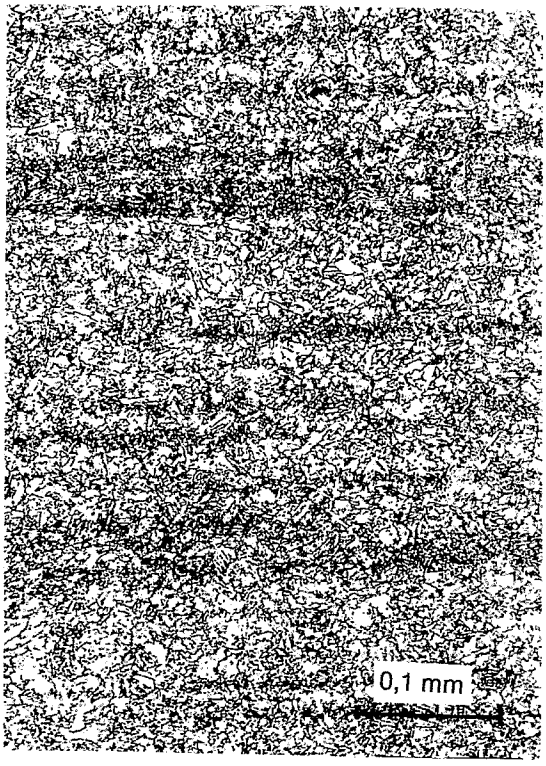


Middle

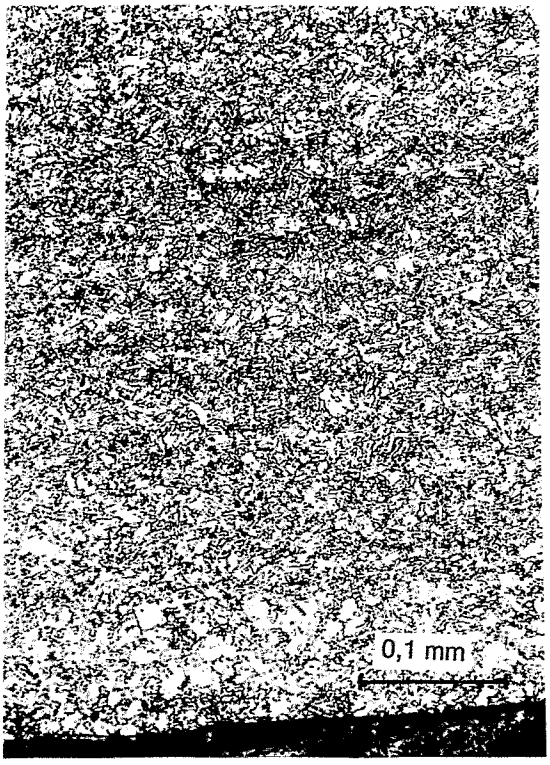


Outside

Fig. 23: Microstructure of sample C2/1, different locations over the wall thickness

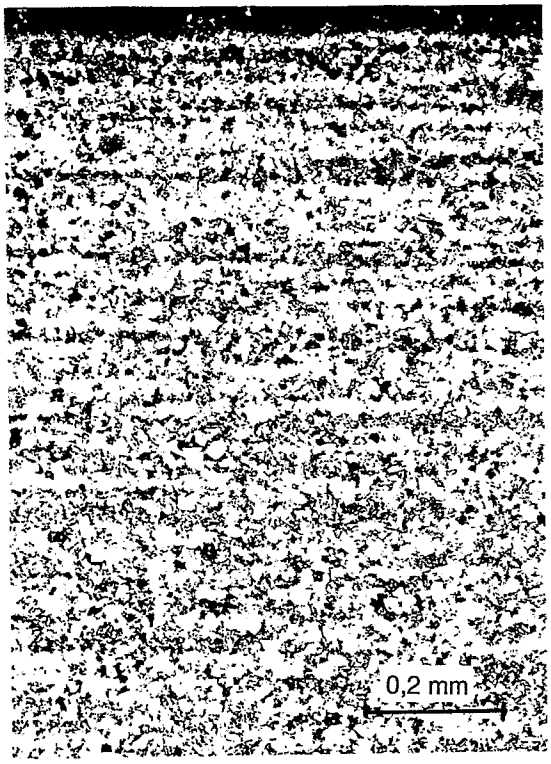


Inside

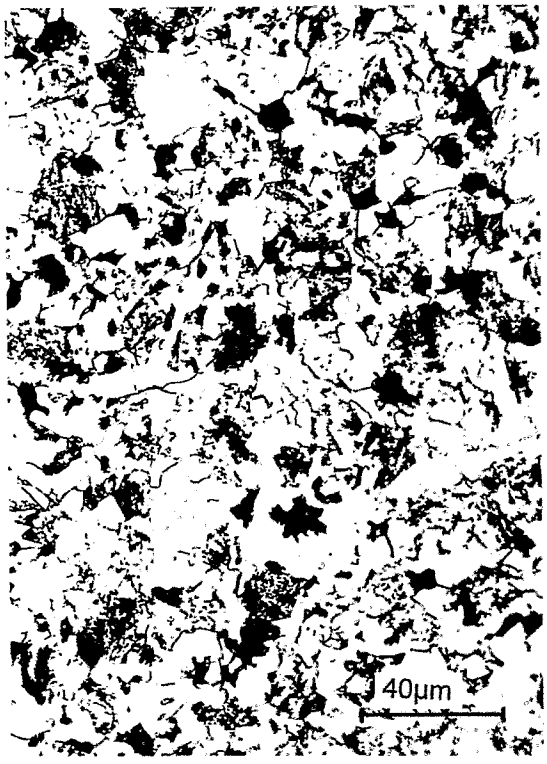


Middle

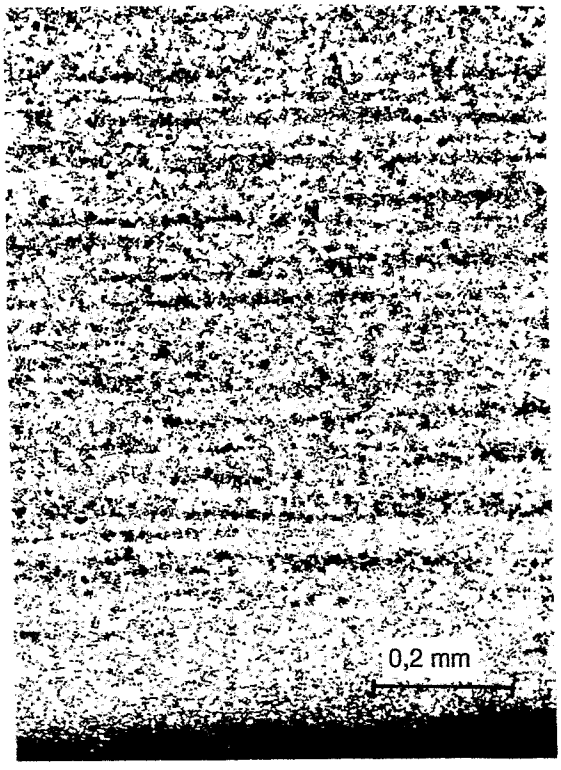


Outside

Fig. 24: Microstructure of sample C2/3, different locations over the wall thickness


Inside

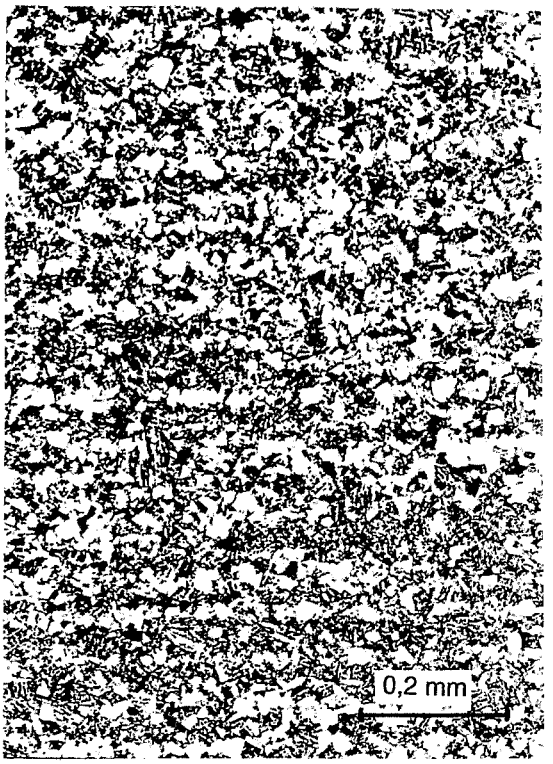


Middle

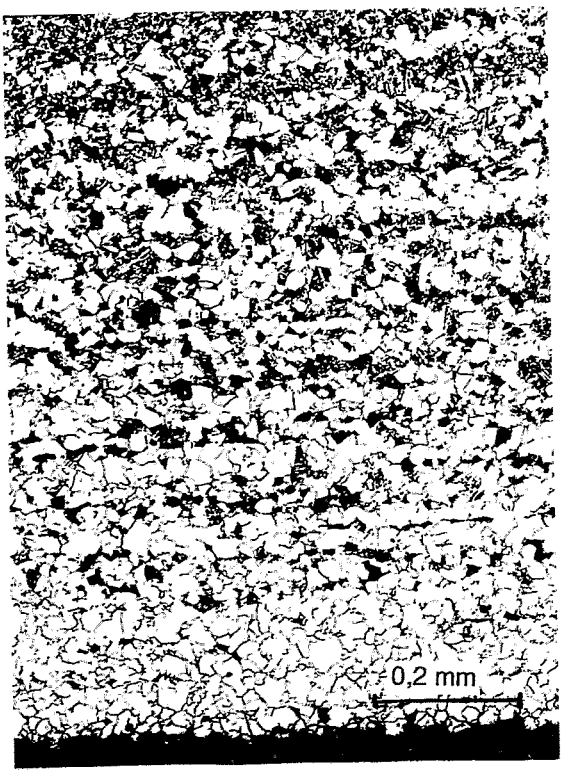


Outside

Fig. 25: Microstructure of sample C2/4, different locations over the wall thickness


Inside

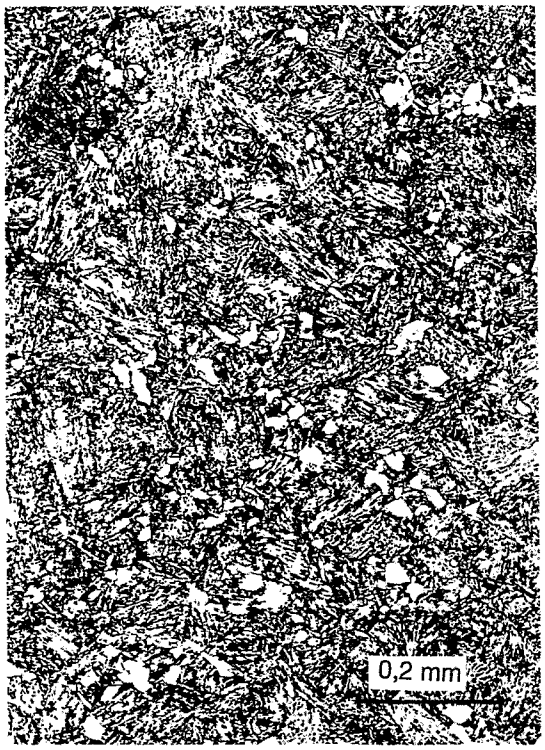


Middle

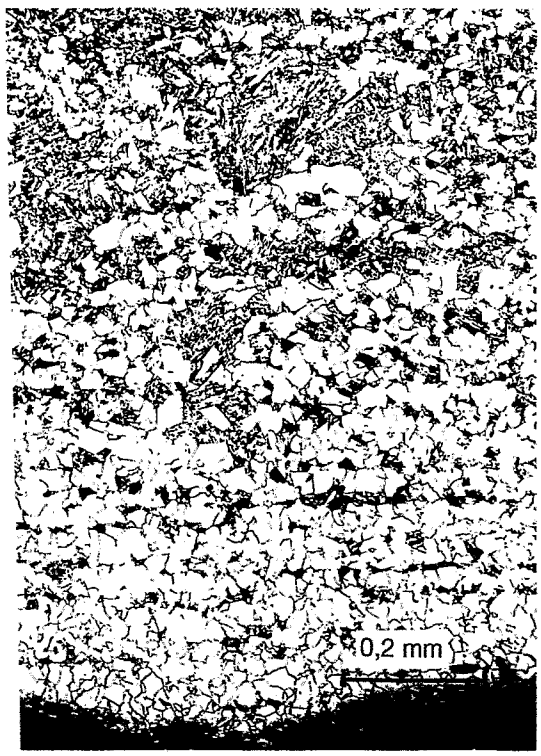


Outside

Fig. 26: Microstructure of sample C2/5, different locations over the wall thickness

Inside

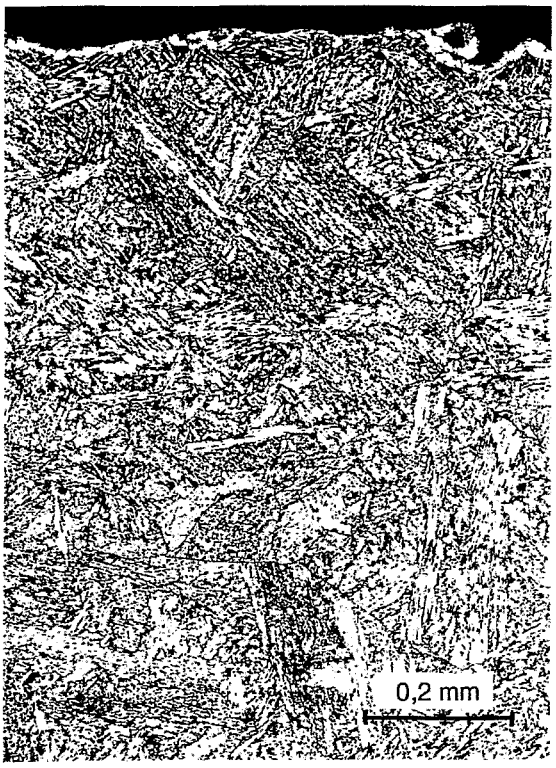



Middle


Outside

Fig. 27: Microstructure of sample C2/6, different locations over the wall thickness

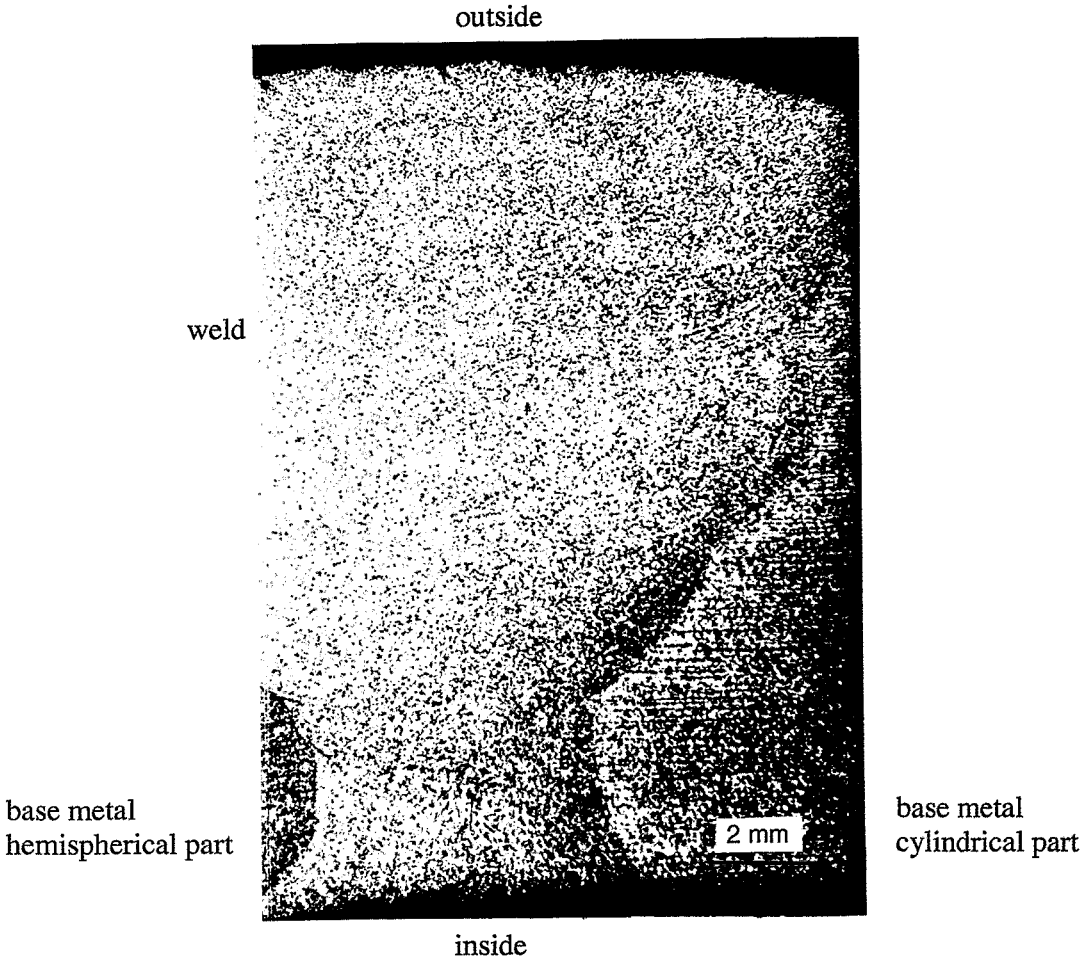


Fig. 28: Macrostructure of sample C2/S, weld and adjacent base metal

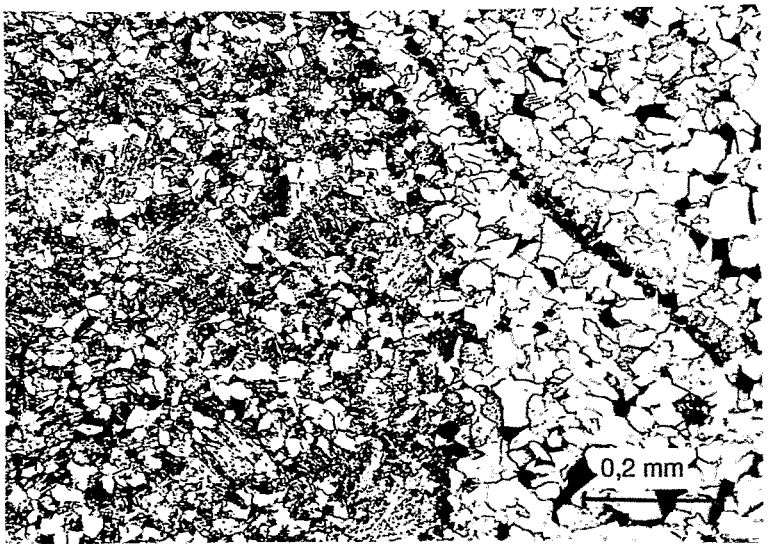


Fig. 29: Microstructure of sample C2/S, weld and base metal of the lower part of the vessel

Inside


Middle

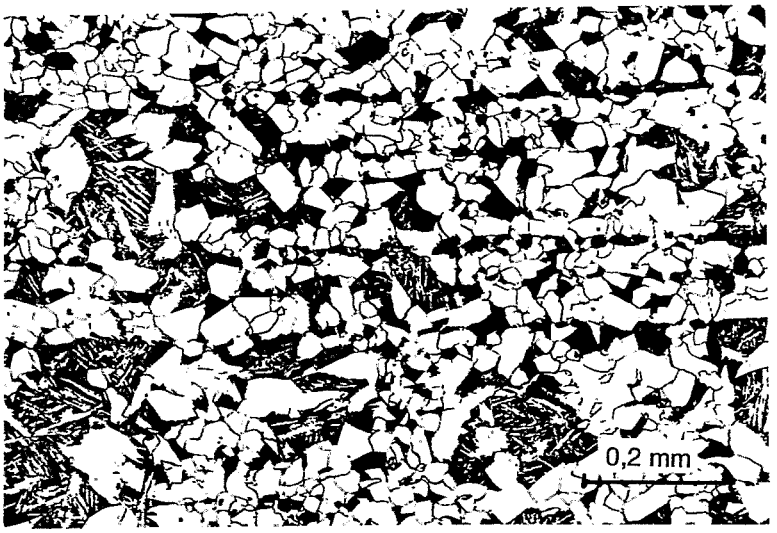


Outside

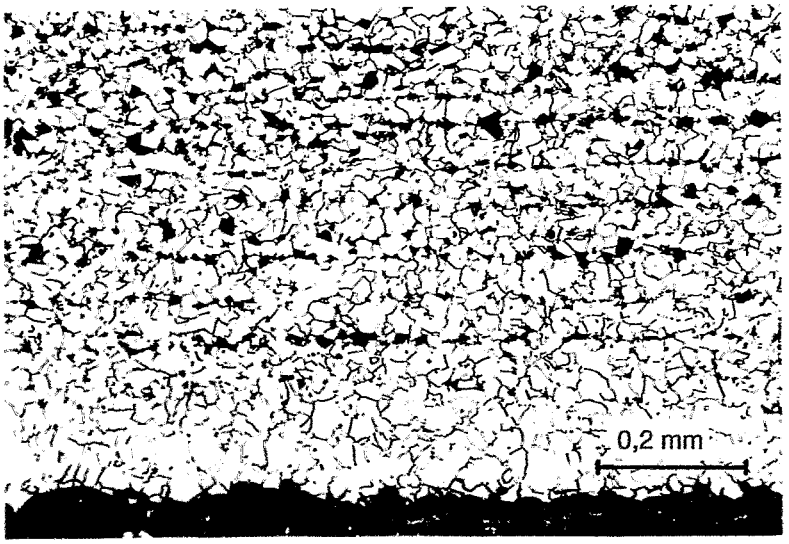


Fig. 30: Microstructure of sample C2/S, base metal of the cylindrical part of the vessel

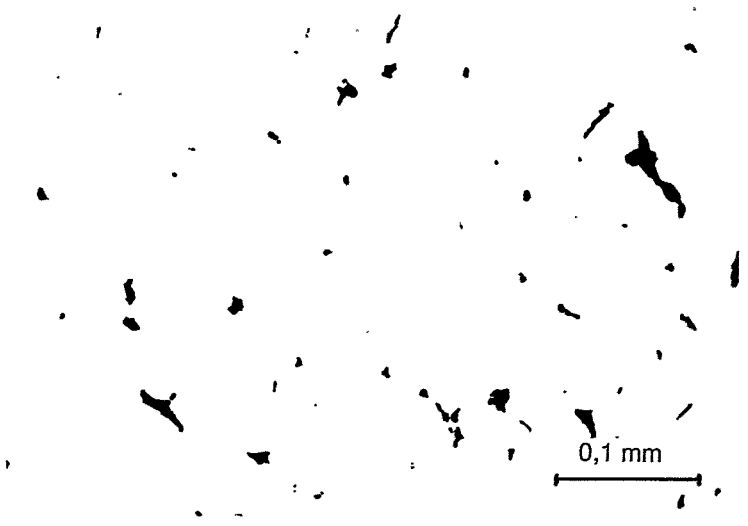


C2/6, sample non etched

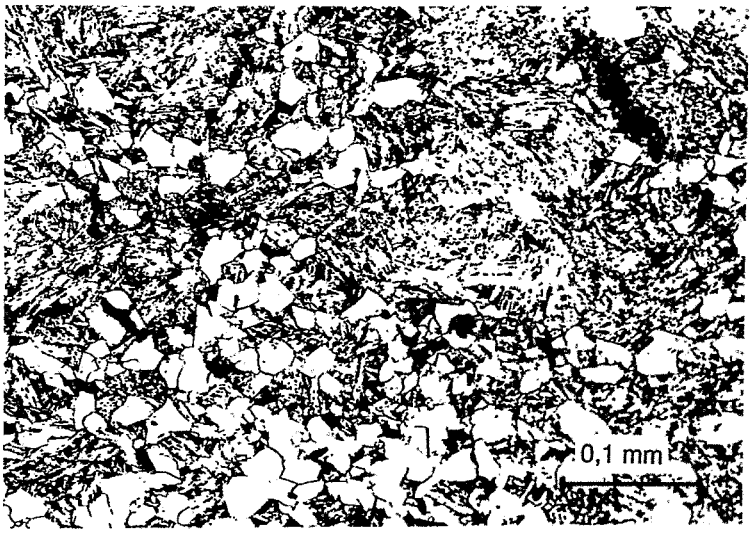


C2/6, sample etched

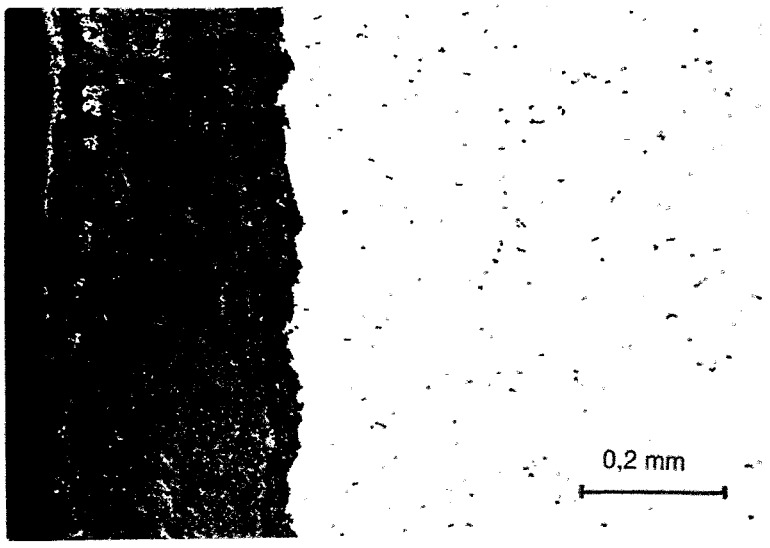


C2/S, sample non etched

Fig. 31: Microstructure of samples C2/6 (top and middle) and C2/S (bottom), unetched (top and bottom) and etched (middle) cross section

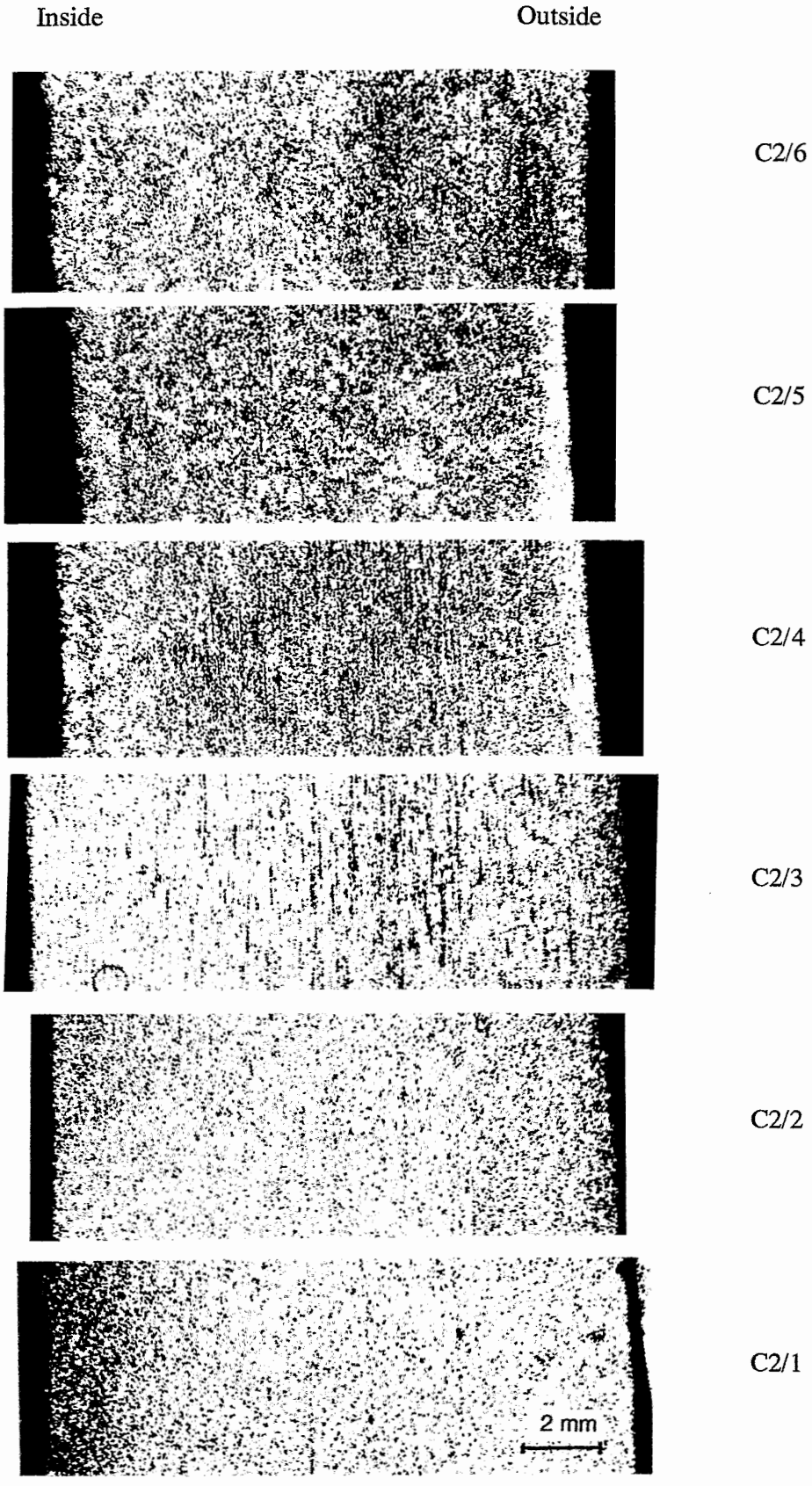


Fig. 32: Macrostructure of the hemispherical part of the vessel, FOREVER-C2

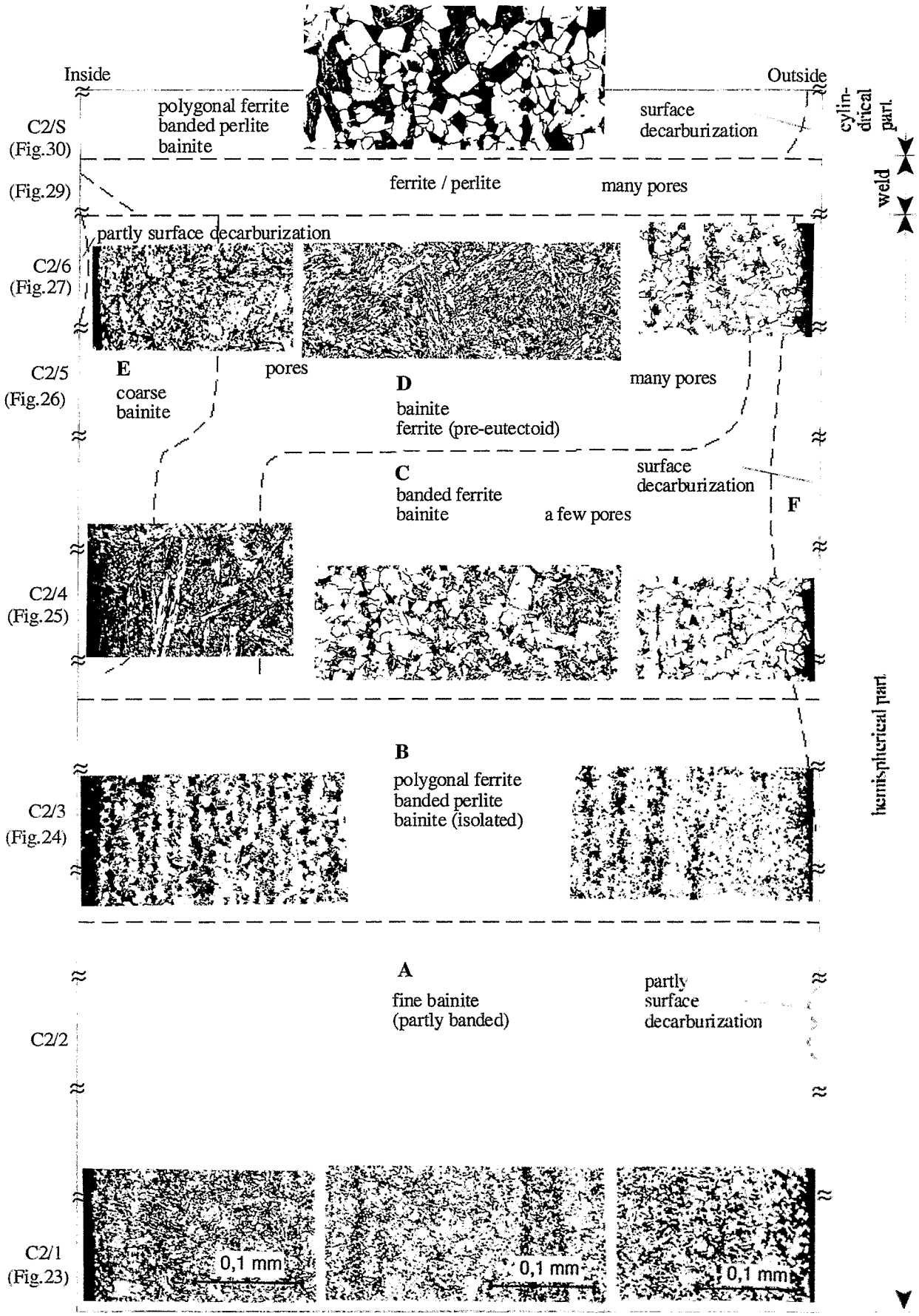


Fig. 33: Map of the characteristic zones of the microstructure over the vessel wall, FOR-EVER-C2 (scale of the microstructures of C2/3 to C2/S: 0.2 mm )

## 5.2 Effects of Annealing

It is assumed that the initial microstructure before annealing is identical to microstructure of the height positions C2/1 and C2/2 as shown in Fig. 23. A very similar microstructure shows Fig. 34 where the microstructure of a sample which is taken from another heat of the French 16 MND 5 steel produced by the same technology is depicted. The same bainitic matrix with pre-eutectoid ferrite and segregated lines appears. After annealing at 800°C the first features of microstructural transformation can be observed (Figs. 35, 36). This concerns above all the microstructure after furnace cooling, where a small fraction of perlite is formed. Figs. 37-39 illustrate that increasing annealing temperature coarsens the ferrite grains and spreads the bands. After air cooling a bainitic microstructure arises (Fig. 40). In this case differences to the initial microstructures are hardly detectable because the annealing procedure is comparable with the final heat treatment during the steel processing. Clearly recognizable microstructural changes appear after annealing at temperatures of 1050°C and higher as shown in Figs. 41-44. There is a microstructural coarsening. Furthermore, even after furnace cooling a large fraction of bainitic islands in the ferritic-perlitic matrix is formed.

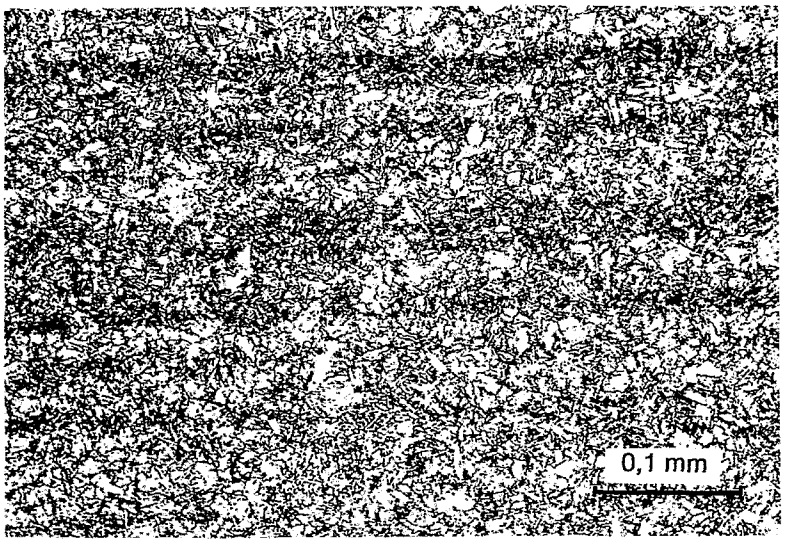


Fig. 34: Microstructure of the French 16 MND 5 steel

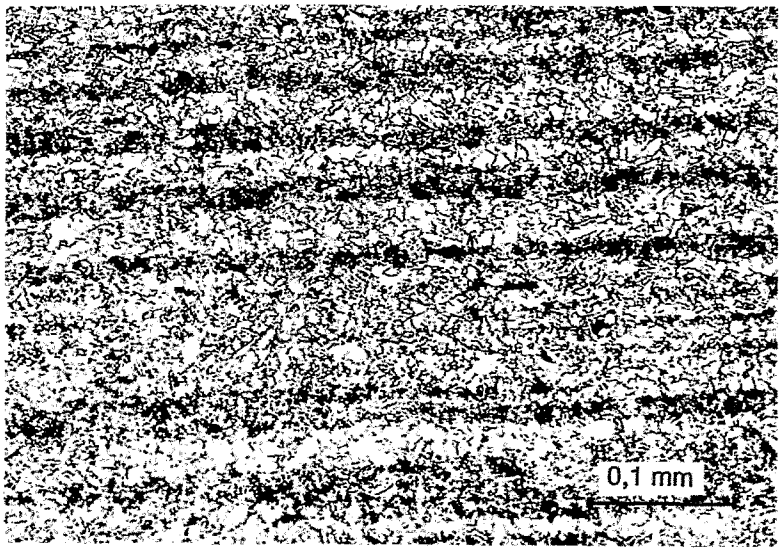


Fig. 35: Microstructure of sample C2/A, annealed: 800°C/2 h, furnace cooling

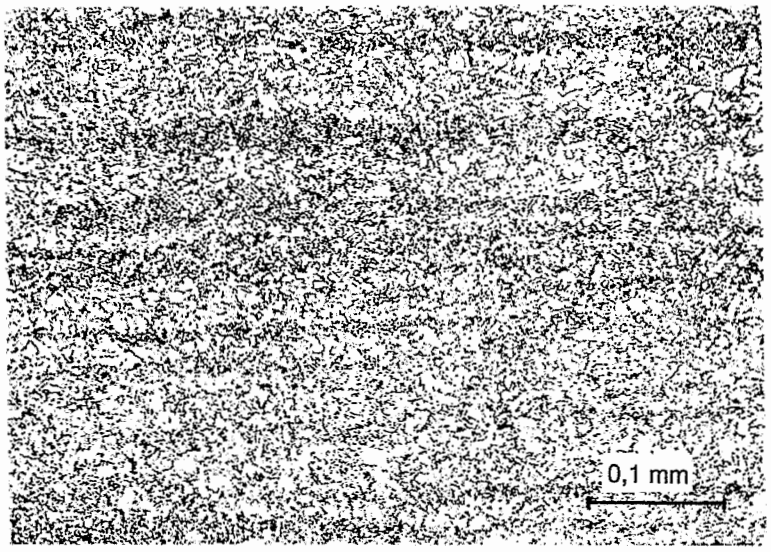


Fig. 36: Microstructure of sample C2/B, annealed: 800°C/2 h, air cooling

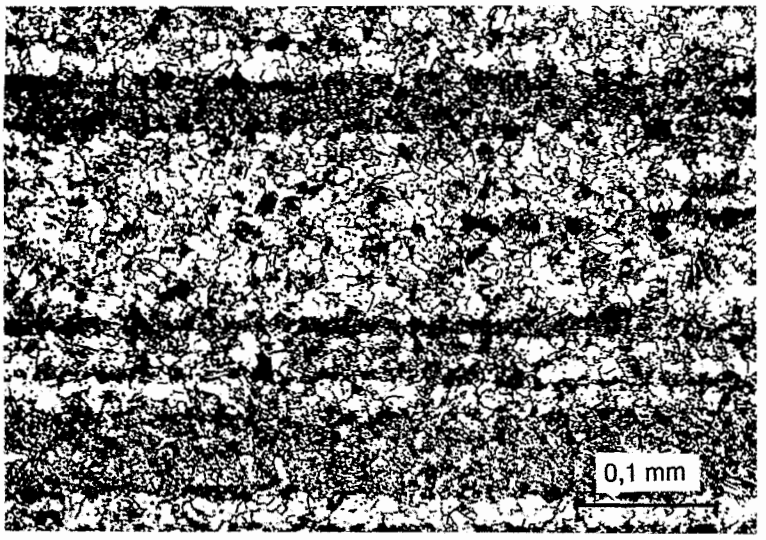


Fig. 37: Microstructure of sample C2/E, annealed: 850°C/2 h, furnace cooling

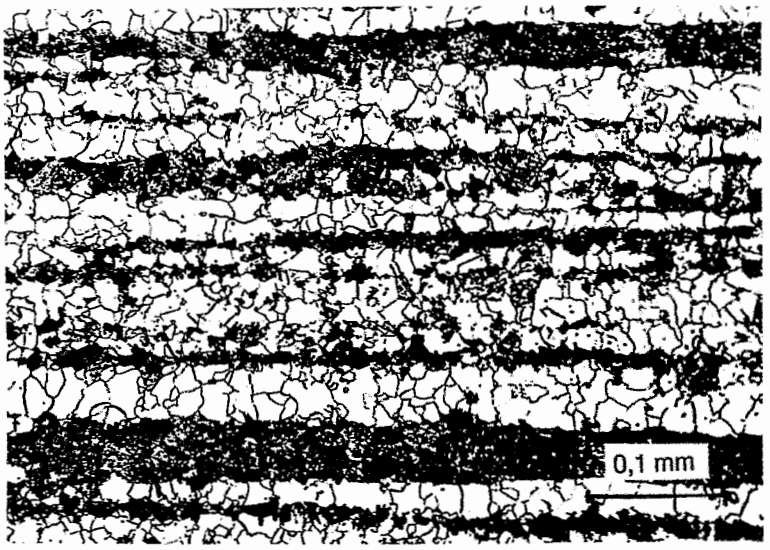


Fig. 38: Microstructure of sample C2/F, annealed: 900°C/2 h, furnace cooling

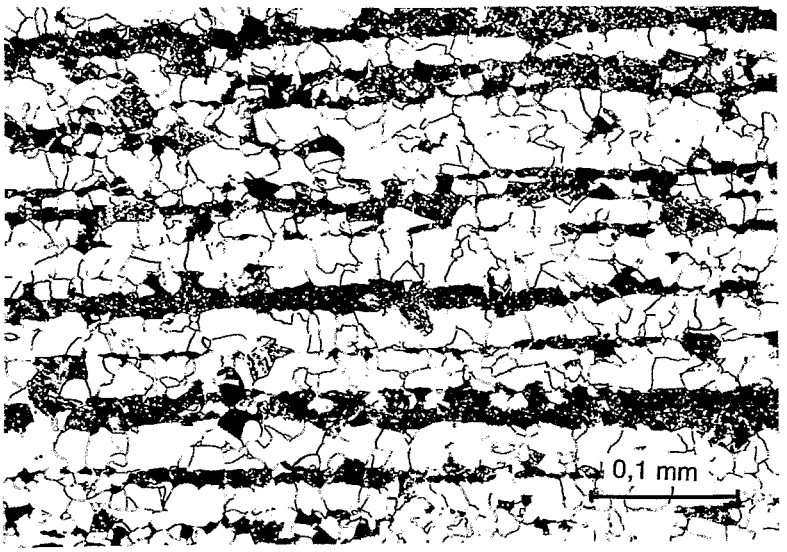


Fig. 39: Microstructure of sample C2/C, annealed: 950°C/2 h, furnace cooling

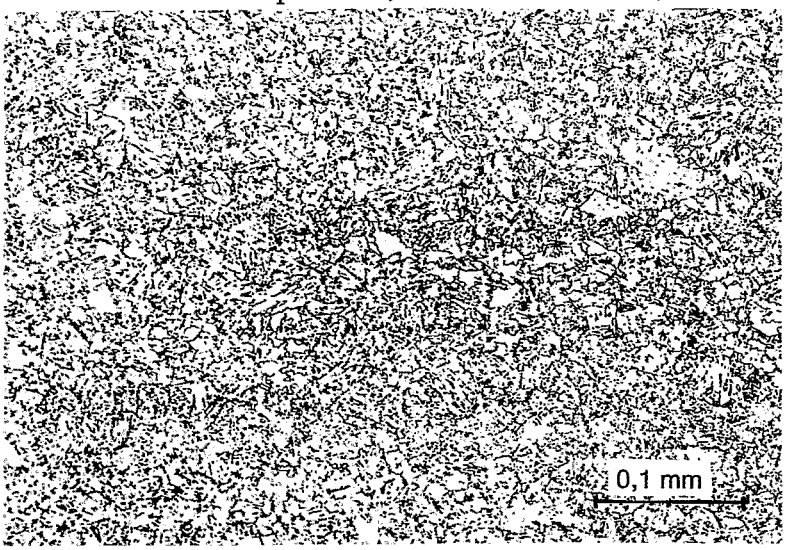


Fig. 40: Microstructure of sample C2/D, annealed: 950°C/2 h, air cooling

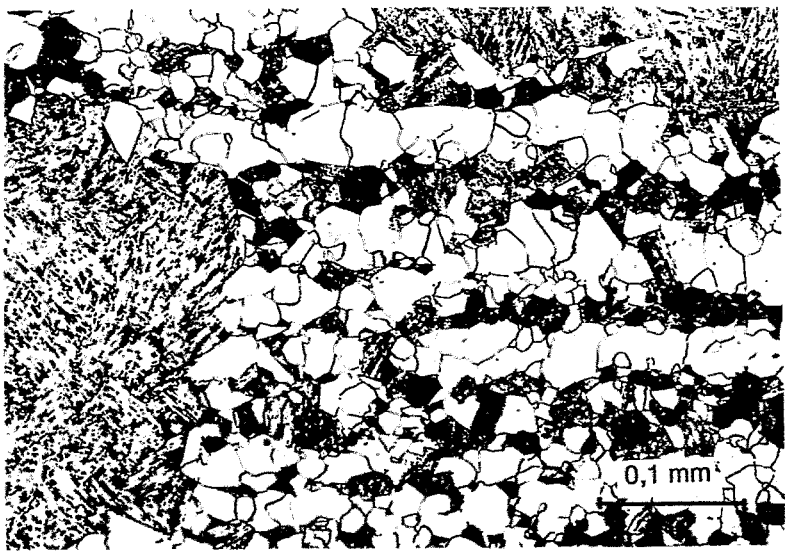


Fig. 41: Microstructure of sample C2/B, annealed: 1050°C/2 h, furnace cooling

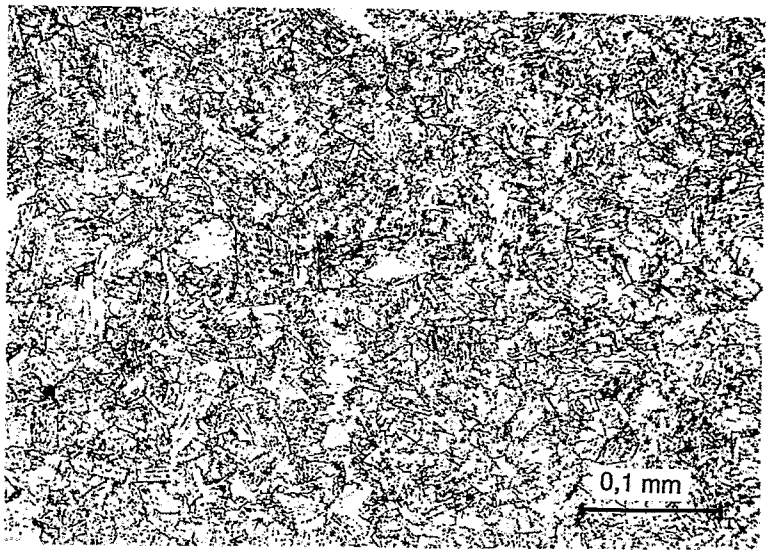


Fig. 42: Microstructure of sample C2/A, annealed: 1050°C/2 h, air cooling


Fig. 43: Microstructure of sample C2/C, annealed: 1100°C/2 h, furnace cooling

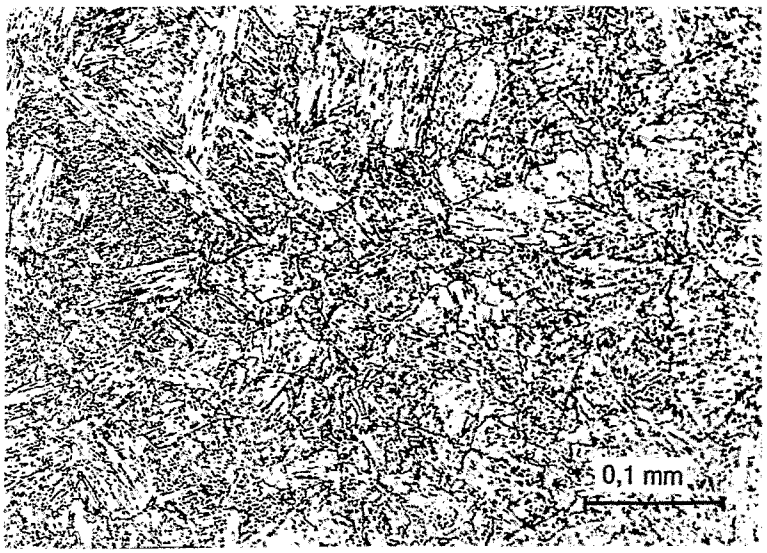


Fig. 44: Microstructure of sample C2/D, annealed: 1100°C/2 h, air cooling

## 5.3 Microhardness

The results of microhardness measurements on the sample C2/6 are depicted in Fig. 45. The microhardness increases within a peripheral layer of < 1 mm to the inside and decreases within a peripheral layer of about 1 mm to the outside.
The microhardness was also measured along a line from the weld to the base metal. The results do not show higher hardness values in the region where the HAZ is expected.

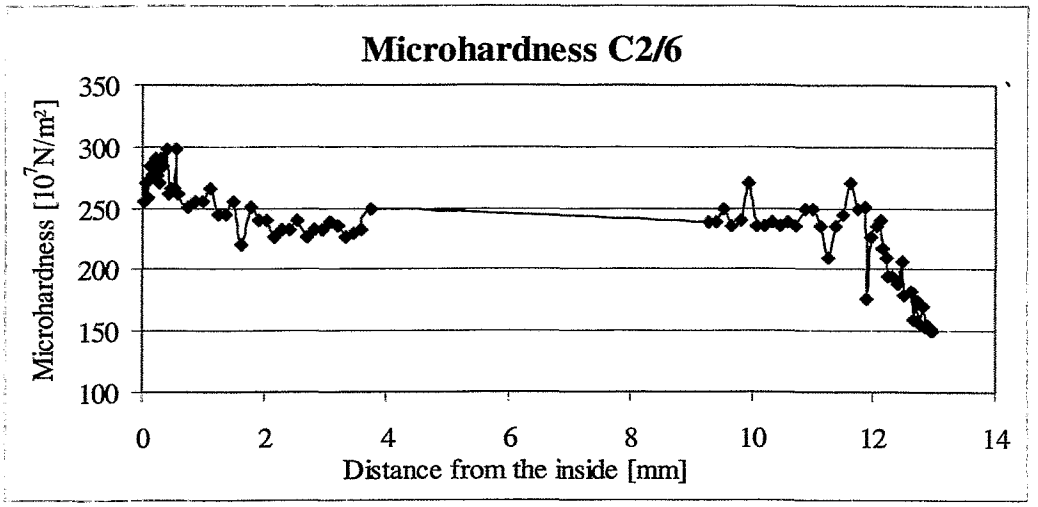


Fig. 45: Microhardness of sample C2/6

## 5.4 Area Fraction of Pores

The area fraction of pores were determined of the samples C2/4, C2/5, C2/6 and C2/S. The results are presented in Fig. 46. The highest fraction of pores occurs at height position of C2/6 and in the weld. In every case the pores are concentrated in a relatively narrow peripheral layer at the outside of the wall. The figure does not reflect the differences in the shape and size of the pores. As mentioned in 5.1 in comparison with the welding region the pores are larger but not so numerous in sample C2/6.

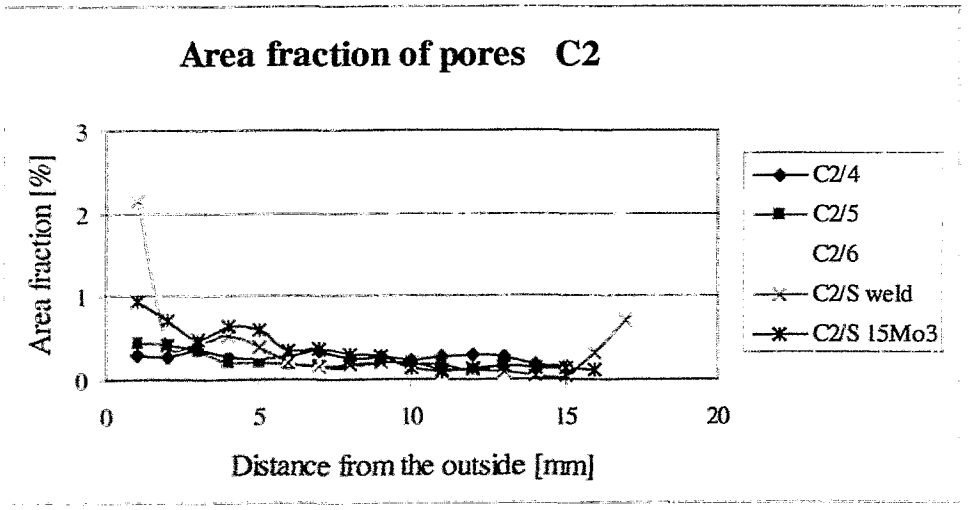


Fig. 46: Area fraction of pores, FOREVER-C2

## 5.5 Microstructure of the Oxidic Melt

Fig. 47 shows the microstructure of the solidified melt. Their vitreous structure is characterized by the two phases CaO and $B_2O_3$ and numerous microcracks.


Fig. 47: Microstructure of the melt, FOREVER-C2

## 6. Discussion

The metallographic examination reveals different microstructural features as summarized in Figs. 12 and 33. The particular problem is the differentiation between the appearances that is characteristic for the initial state and the features induced by the experiment.

The hemispherical lower heads of the vessel were produced from a rolling plate of the French 16 MND 5 steel for FOREVER-C2 and of the German 15 Mo 3 steel for FOREVER-C1. Only for the 16 MND 5 steel there is a sample in the as-received state although it is taken from another heat and is not effected by the warm-pressing procedure. As one can see in Fig. 34, the microstructure consists of bainite what is typical for the reactor pressure vessel material. The bainitic microstructure of the lowest part of the hemispherical head of the FOREVER-C2 vessel (Fig. 23) is comparable with the microstructure in Fig. 34. It seems to represent the state after processing and does not be effected by the temperature regime during the experiment. This microstructure covers the whole wall thickness at the positions C2/1 and C2/2 (zone A according to Fig. 33).
The situation is not so unambiguous for the FOREVER-C1 experiment. In this case there is no sample which represents the as-received state. The microstructure of rolling plates made from 15 Mo 3 and without additional heat treatment is a typically polygonal ferritic matrix with banded perlite. Just this microstructure appears in all samples from the lower head but its extent changes over the height position. It occurs on the interior half of the wall at the positions C1/1 and C1/2 (Fig. 4), covers almost the whole cross section of sample C1/3, and is located on the outside half of the wall at the higher positions with a minimum extension at C1/5. The ferrite-banded perlite microstructure is also typical for the cylindrical part of the vessel and can be classified as the initial state. Additionally, some microstructural features are probably caused by the hot-pressing to the hemispherical shape. This concerns the fine-grained ferrite zone at the inside and the duplex ferrite grain-banded perlite zone near the outside at the positions C1/1 – C1/3.
The uneffected initial state also shows the welded joint of the FOREVER-C1 samples. The weld metal has the typical solidification structure with columnar or elongated grains. Furthermore, the HAZ is not changed.

Clearly visible microstructural changes appear near the inside at the positions C1/4 to C1/6 after the FOREVER-C1 experiment. Here the banded distribution of the perlite is vanished and a randomly distributed fine-grained ferrite-perlite mixture is created. The region has its largest extent at the position C1/5 where more than the half of the wall thickness is covered by this microstructure.
Such microstructural changes appear first at temperature above $A_{C3}$. According to the CCT diagram of 15 Mo 3 steel (Fig. 1) the $A_{C3}$ temperature is 850°C – 865°C. A valuable hint provides the comparison with the annealing experiments. The microstructure after annealing at 900°C (Fig. 17) is comparable with the mentioned microstructure. Higher annealing temperatures produce grain growth and, thus, coarse ferrite grains after the austenite-ferrite retransformation. As such appearances are not observed, temperatures above 950°C did not occur or only for a short time. This suggests that the maximum temperature during experiment was about 900°C at the wall inside and the height position C1/5. The maximal external temperatures was < 850°C as there is no microstructural transformation at the outside of the vessel wall. (The pure coarse-grained ferrite at the outside is caused by another effect as explained later.)

A stronger effect of the experiment shows the microstructure of the FOREVER-C2 vessel. During the course of this experiment the microstructure is clearly changed over a region

reaching from the height position C2/3 up to base metal of the upper part of the vessel near the welding seam. The micorstructural changes have both a gradient along the height position and over the wall thickness. Here one can differ 4 zones (designated B,C,D and F in Fig. 33) which characterize 4 temperature-cooling rate levels.

The microstructure of zone B (height position C2/3, Fig. 24) must be caused by temperatures above $A_{C3}$ and a slow cooling rate. It consists of polygonale ferrite, banded perlite and only isolated bainite and covers almost the whole cross section. Similar microstructures, but clearly coarser, were obtained by annealed samples (850°C/900°C/950°C, furnace colling, Figs. 37-39). The higher the annealing temperatures the larger are the grains. Furthermore, the annealing time coarsens the grains as well although the effect was not investigated in this work. As the exposition time of FOREVER-C2 was about 6 times longer than the time of the annealing experiments, one can conclude that the temperature during FOREVER-C2 is not higher than approx. 850°C at this position. A further finding bears out that the temperatures within the wall did not exceed the $A_{C3}$ temperature. Within the ferrite grains or at the boundaries of the ferrite there are small areas coloured dark gray (Fig. 24). Investigation by EDX/SEM shows that the small areas do not have a considerably different composition than the ferritic matrix as can be recognized by Fig. 48. The results of the EDX analysis are quite identical for the spectrum 1 in Fig. 48 measured in a ferritic matrix grain and for the spectrum 2 from the area at the grain boundary. It is assumed that the steel transformed only partially to austenite while the largest part of ferrite was retained. The ferrite which was formed during the subsequent cooling from the austenite has a little changed composition and, thus, a changed etching response.

Another modification of the microstructure is observed from the height position C2/4 up to the weld. At the wall inside a zone (E according to Fig. 33) of very coarse bainite was generated and its extent amounts to 1 mm at positions C2/4 and up to 2 mm at C2/6 (Figs. 25-27). The formation of this zone requires two conditions: a) a relatively fast cooling rate and b) a temperature considerably above $A_{C3}$. The highest temperature during FOREVER-C2 was here and reached approx. 1100°C. The following region into the wall thickness (zone D) at the positions C2/4 – C2/6 consists of a finer bainite and pre-eutectoid ferrite. The ferrite is arranged like clusters. The extension of the region reaches from 1-2 mm (C2/4, Fig. 25) up to 12 mm (C2/6, Fig. 27). Subsequently, it follows a region (zone C) of banded ferrite and bainite, which extends up to the wall outside. It is wide at position C2/4 (9 mm) and very narrow at position C2/5 or C2/6 (0,5 mm). For the microstructure of zone C and D the annealing experiments do not provide analogous results, but one can conclude that the temperature was higher than $A_{C3}$ ( 870°C) and lower 1050°C.

The microstructure of the weld (Fig. 29) consisting of ferrite and perlite is not typical for a welded structure and there is no HAZ. For the last the uniform course of the microhardness at the transition between weld and base metal is an additional indication. Both phenomena prove that temperatures reached considerably more than $A_{C3}$ ( 870°C).

The results of the annealing experiments can only be considered with a proviso because the composition and the initial state of the weld and the base metal used for the annealing experiments were different. A rough estimation suggests a temperature approx. between 1000°C and 1050°C in the weld.

A microstructural transformation also shows the 15 Mo 3 steel of the upper cylindrical part of vessel near the weld. The microstructure consists of coarse-grained polygonal ferrite, banded perlite and inclusions of coarse bainite. The grain size and the fraction of bainite increase with decreasing distance to the wall inside. This feature indicates a complete transformation of the initial microstructure to austenite during the experiment. The grain growth is produced by higher annealing temperatures. The annealing experiments with samples of 15 Mo 3 steel from the FOREVER-C1 experiment provide similar structures (Figs. 19, 20). For example the

microstructure after annealing at 1050°C is comparable with the inside microstructure. However, the characteristic of the bainite points to a relatively fast cooling rate.

Information about the thermo-mechanical loads provides the presence of creep pores. Creep pores are only visible in samples of the FOREVER-C2 experiment. Thus, in FOREVER-C1 the primary creep stage is not exceeded and the creep damaging can be neglected.
Numerous pores appears at the height positions C2/4 to C2/6, in the weld and in the cylindrical part near the weld. Shape, size and quality of pores change over the wall thickness and the height position of the vessel. The highest concentration are observed at the outside of the vessel close to the lower fusion line in the base metal. However, the size and shape of the pores differ for the base metal and the weld. The base metal possesses larger and crack-like cavitations, what indicates that at least the transition between secondary and tertiary creep stage was reached. The volume fraction of pores seems to correlate with the temperature related to the height position whereas the course over the thickness depends additionally of the mechanical loading conditions. Thus, the volume fraction is higher at the outside than the inside although the course of temperature is inverted.

Some microstructural phenomena are caused by environmental effects. Surprisingly, there is hardly an interaction between vessel and oxidic melt. Only along a short section of the hemispherical head of vessel for FOREVER-C1 a very small surface layer with increased boron content can be proven (Fig. 21). FOREVER-C2 does not, however, show any reaction in spite of the higher thermal loads.
As expected a strong surface oxidation occurs at the outside due to the reaction with the air atmosphere. The argon-containing internal vessel atmosphere effects the formation of a thin oxide layer. These effects are not considered in detail in this paper. An typical example of the oxide layer is shown in Fig. 31 (bottom). It is estimated that the influence of the oxidation of the wall thickness reduction is irrelevant.
Eventually, the gas atmosphere causes decarburization of a surface layer. The effect is observed at the inside as well as at the outside of wall but more effective at the outside. The largest layer is formed at the positions C1/4 – C1/6 or C2/4 – C2/6 respectively and reaches value of almost 1 mm. The decarburized layer is characterized by a pure ferritic microstructure. Depending on the temperature the ferrite grains are enlarged. The inside wall is protected against oxidation due to the argon atmosphere and the melt. Thus, a decarburization is hardly relevant.
The decarburization process takes place at temperatures above $A_{C1}$ and depends on temperature, time and carbon activity in a complicated manner. Obviously, the decarburized zone width also characterizes the temperature course over the height position but it cannot be quantified because many factors are of influence additionally. However the mechanical properties are changed in the decarburized layer as the reduction of the microhardness at the outside, depicted in Fig. 45, proves. For a long duration of exposition, the effect has to be also considered for numerical simulation.

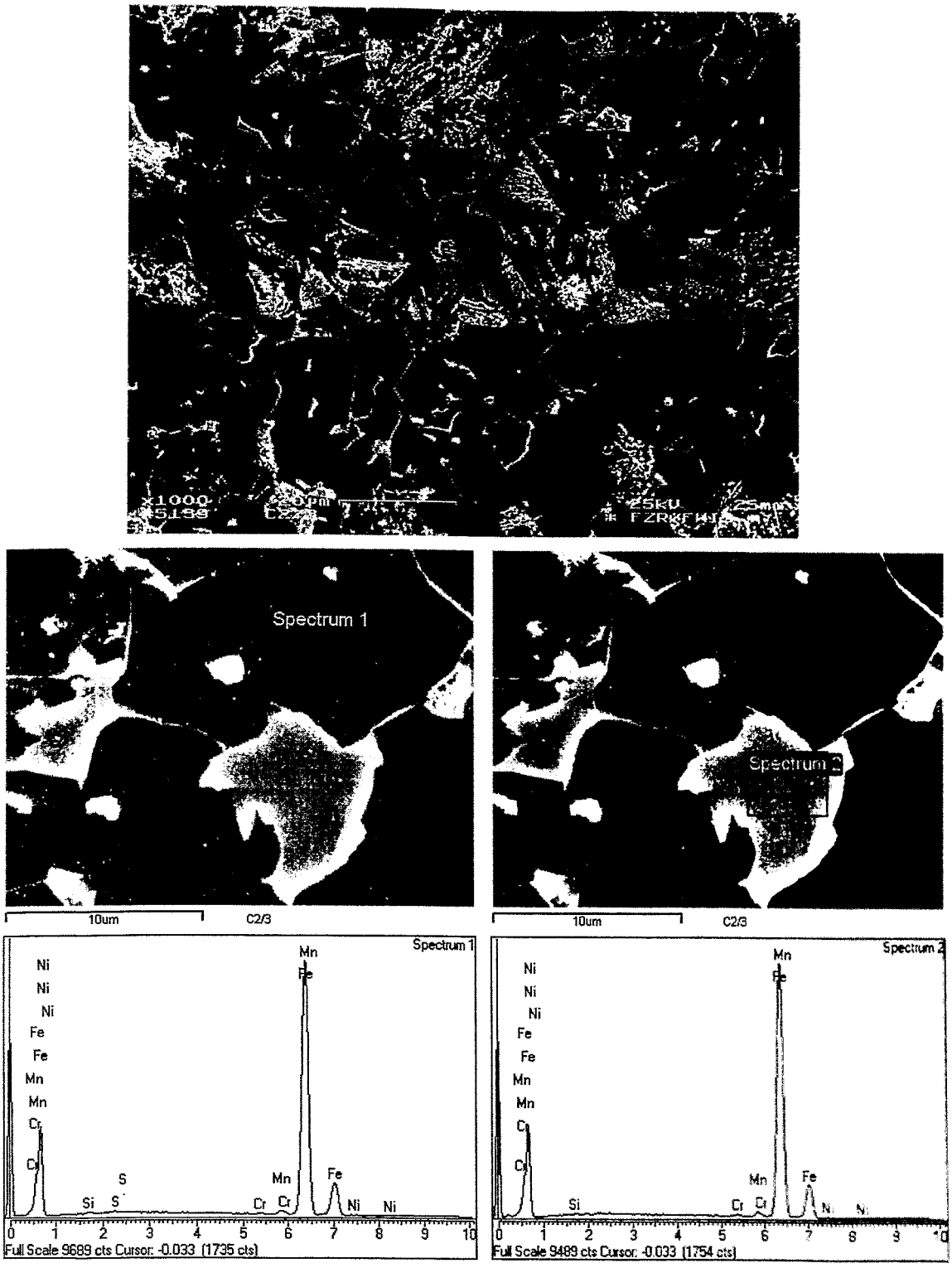


Fig. 48: Microstructure of sample C2/3, SEM photograph (top) and Energy Dispersive X-ray Analysis (bottom)

## 7. Conclusion

The FOREVER-C experiments investigate the vessel deformation and creep behaviour under thermal attack by an oxidic melt pool. The high temperatures during the test and the environmental conditions affect the behaviour of the vessel material.
Metallographic examination of samples taken from different positions of the vessel wall was performed in order to detect experiment-induced microstructural changes. Additionally, annealing experiments with subsequent microstructural investigation, microhardness measurements, ion micropobe analysis and scanning electron microscopy with energy dispersive X-ray analysis of selected samples were also carried out.
The result of the metallographic examination is a two-dimensional profile of the microstructure over the wall thickness and along the height position. Regions of microstructural appearances that are correlated to special transformation temperature or environmental effects could be defined. In this way the region of highest thermal loads could be identified and the axial and radial thermal gradient could be proven. The maximum temperature occured during the experiments was clearly higher for FOREVER-C2 than -C1. FOREVER-C2 also has a higher thermo-mechanical load. As the result of this, creep pores are formed at highly loaded positions. They indicate a remarkable creep damage. Furthermore, the metallographic examination also identifies interactions between the environment and vessel material which are not very relevant for the vessel response during the test. There is hardly a reaction between the oxidic melt and the vessel wall.
The metallographic examination has proven to be a valuable tool for the analysis of the conditions and the sequence of the FOREVER experiments. However, they must be supplement by annealing experiments under simulated test conditions and with the same material. Moreover, the material state before starting the experiment must be well-known. Under these circumstances the temperature regime and the temperature profile can be determined with an error of ± 20°C. Finally, the failure mode can be characterized and hints to the design of further experiments can be derived.

## References


[1] R.R. Nourgaliev, A. Karbojian, T.N. Dinh, B.R. Sehgal
FOREVER Experiments on Thermal and Mechanical Behavior of a Reactor Pressure Vessel during a Severe Accident. Technical Report-1. FOREVER-C1 test, MVI Project Research Report, Stockholm 1998

[2] E. Altstadt, H.-G. Willschütz
Development of an Integral Finite Element Model for the Simulation of Scaled Core-Meltdown Experiments, Forschungszentrum Rossendorf, Wissenschaftlich-technische Berichte, FZR-292, April 2000

[3] R.R. Nourgaliev, A. Karbojian, A. S. Theerhan, B.R. Sehgal
Failure of Reactor Vessel Retention FOREVER-C2 Test and Analysis
Melt-Structure-Water Interactions, MSWI Project, Research Report, June 19, 1999

[4] B.R. Sehgal, R.R. Nourgaliev, T.N. Dinh, A. Karbojian
FOREVER experiment program on reactor pressure vessel behaviour and core debris Retention, Proceedings of the 15th International Conference on Structural Mechanics in Reactor Technology (SmiRT-15), Seoul, Korea, August 1999

[5] Certificat of Heat Treatment 02174, 6.2.98
Finn Heat, Pitea, Sweden

[6] G. Münch, G. Stenzel, D. Naundorf, A. Lässig
Zeit-Temperatur-Umwandlungs-Diagramme, Edelstahlwerke Freital

[7] G. Kalwa, E. Schnabel
Wärmebehandlung und Eigenschaften dickwandiger Bauteile aus warmfesten Röhrenstählen
VGB Kraftwerkstechnik 58 Heft 8 (August 1978) 604 - 613

[8] F. Herrmann, D. Grambole
New Rossendorf Nuclear Microprobe
Nucl. Instr. and Meth. B 104 (1995) 26